

Response to Associate Editor Comments for BG-2017-217

Comments to the Author:

Dear Suzanne, Cara,

Thank you for your detailed replies to both referee reports. I have now gone through both sets of author replies and the revised version of your manuscript, and feel you have thoroughly and convincingly addressed the suggestions and comments made. Considering also the favourable recommendations by both reviewers, I am therefore pleased to accept your revised version for Biogeosciences.

I would like to make 2 additional suggestions to consider before uploading the final version of your files:

-In the abstract, I feel the conclusions concerning the different water sources (best explored in section 5.3 but relevant not also for DOC concentrations) would be worth including more explicitly, i.e. a key message would be that different water sources contribute to the outflow of the slumps, that these have different DOC concentrations and characteristics (and age), but that the overall decrease in DOC concentrations is not simply a mixing of different sources but that other DOC losses (the proposed mechanism being sorption to particles) also occur.

-I would be strongly in favour (as for all manuscripts) to provide the full data as an electronic supplement. I feel the dataset should be relatively straightforward to organize in a way that is clear to potential users - and that making the full data publicly available will increase their potential value (e.g. use in larger data syntheses).

With best regards
Steven Bouillon

Dear Steven,

Thank you for your kind comments – we are excited to have our paper accepted with minor revisions in Biogeosciences! In response to your comments, we have reworked the abstract in an attempt to more clearly outline the findings in Section 5.3. We also now include our data in Supplemental Tables S1 and S2.

In addition to the changes outlined above, all authors have re-read the manuscript one last time, which has resulted in some editorial changes. The updated manuscript has been submitted as a tracked changes PDF (attached below), and as a clean PDF. The edits made in this round were all stylistic, and none of them affect the changes that were made in response to the reviewers' comments.

Best regards,

Suzanne Tank (on behalf of Cara Bulger, and Steve Koklelj)

1 **Retrogressive thaw slumps temper dissolved organic carbon delivery to streams of the Peel Plateau,**
2 **NWT, Canada**

3

4 Cara A. Bulger¹, Suzanne E. Tank¹, and Steven V. Kokelj²

5

6 ¹Department of Biological Sciences, University of Alberta, Edmonton, AB, T6G 2E9, Canada

7 ²Northwest Territories Geological Survey, Government of the Northwest Territories, Yellowknife, NT,

8 X1A 1K3, Canada

9 *Correspondence to:* Cara A. Bulger (cara.bulger@gmail.com)

10

11

12 **Abstract**

13 In Siberia and Alaska, permafrost thaw has been associated with significant increases in the delivery of
14 dissolved organic carbon (DOC) to recipient stream ecosystems. Here, we examine the effect of
15 retrogressive thaw slumps (RTS) on DOC concentration and transport, using data from eight RTS features
16 on the Peel Plateau, NT, Canada. Like extensive regions of northwestern Canada, the Peel Plateau is
17 comprised of thick, ice-rich tills that were deposited at the margins of the Laurentide Ice Sheet. RTS
18 features are now widespread in this region, with headwall exposures up to 30 m high, and total
19 disturbed areas often exceeding 30 ha. We find that intensive slumping on the Peel Plateau is universally
20 associated with decreasing DOC concentrations downstream of slumps, even though the composition of
21 slump-derived dissolved organic matter (DOM; assessed using specific UV absorbance and slope ratios)
22 is similar to permafrost-derived DOM from other regions. Comparisons of upstream and downstream
23 DOC flux relative to fluxes of total suspended solids suggest that the substantial fine-grained sediments
24 released by RTS features may sequester DOC. Runoff obtained directly from slump rillwater, above entry
25 into recipient streams, indicates that the deepest RTS features, which thaw the greatest extent of
26 buried, Pleistocene-aged glacial tills, release low concentration DOC when compared to paired
27 upstream, un-disturbed locations, while shallower features, with exposures that are more limited to a
28 relict Holocene active layer, have within-slump DOC concentrations more similar to upstream sites.
29 Finally, fine-scale work at a single RTS site indicates that temperature and precipitation serve as primary
30 environmental controls on above-slump and below-slump DOC flux, but that the relationship between
31 climatic parameters and DOC flux is complex for these dynamic thermokarst features. These results
32 demonstrate that we should expect clear variation in thermokarst-associated DOC mobilization across
33 Arctic regions, but that within-region variation in thermokarst intensity and landscape composition is
34 also important for determining the biogeochemical response. Geological and climate legacy shape the
35 physical and chemical composition of permafrost, and thermokarst potential. As such, these factors
36 must be considered in predictions of land-to-water carbon mobilization in a warming Arctic.

Deleted: changes in

Deleted: within slump features

Deleted: have the lowest runoff DOC concentrations

Deleted: . In contrast,

Deleted: striking

Deleted: other

Deleted: factors is

Deleted: An understanding of landscape and climate history, permafrost genesis, soil composition, the nature and intensity of thermokarst, and the interaction of these factors, is critical for

Deleted:

Deleted: ing changes in

50 **1. Introduction**

51 Anthropogenic climate change is significantly affecting the Arctic cryosphere (IPCC, 2014).
52 Temperature increases in circumpolar regions are predicted to be at least 40 % greater than the global
53 mean, while precipitation is also expected to increase significantly in most locations (IPCC, 2014). The
54 resulting degradation of permafrost is forecast to have wide-ranging effects, because thawing has the
55 potential to greatly alter the physical, chemical, and biological functioning of landscapes (Frey and
56 McClelland, 2009; Khvorostyanov et al., 2008a, 2008b; Kokelj et al., 2017b; Schuur et al., 2008, 2013). In
57 particular, permafrost acts as a long term storage medium for solutes and sediments, and as a barrier to
58 the participation of permafrost-sequestered constituents within active biogeochemical cycles (Frey and
59 McClelland 209; Vonk et al. 2015b). Consequently, permafrost thaw can enhance linkages between
60 terrestrial and aquatic systems, via increased transport of terrestrial compounds from land to water
61 (Kokelj et al. 2013; Tanski et al., 2016; Vonk et al., 2015b). Given that circumpolar stores of permafrost
62 carbon are estimated to be almost double that of the atmospheric carbon pool (Hugelius et al., 2014),
63 there is great potential for large increases in carbon mobilization as a result of permafrost thaw (Schuur
64 et al., 2015). Within this context, the mobilization of dissolved organic carbon (DOC) from previously
65 frozen soils is of particular interest, because DOC acts as the primary substrate for the microbially-
66 mediated mineralization of organic carbon to carbon dioxide (Battin et al., 2008), and serves as the
67 primary vehicle for the delivery of terrestrial carbon to the Arctic Ocean (Dittmar and Kattner, 2003;
68 Holmes et al., 2012; Spencer et al., 2015). As a result, the implications of thaw-mediated DOC
69 mobilization may range from effects on the permafrost-carbon feedback, to the ecological and
70 biogeochemical functioning of streams, rivers, and the nearshore ocean (e.g. Fritz et al. 2017; Tank et
71 al., 2012b; Vonk et al., 2015b).

72 Permafrost thaw can manifest in many different forms, ranging from an increase in active layer
73 thickness and terrain subsidence, to thermokarst features that significantly reconfigure the physical
74 structure of landscapes (Kokelj and Jorgenson, 2013). Of these, thermokarst has the potential to rapidly

Deleted: Canadian

Deleted: Arctic

Deleted: many

Deleted: northern

Deleted: permafrost

Deleted: while also serving

Deleted: the

82 expose significant quantities of previously-frozen soils to biological and chemical processing (Abbott et
83 al., 2014, 2015; Malone et al., 2013; Tanski et al. 2017). One of the most conspicuous manifestations of
84 thermokarst is the retrogressive thaw slump (RTS; Fig. 1), which develops as a result of mass wasting in
85 ice-rich glacial deposits across northwestern Canada, Alaska, and western Siberia (Kokelj et al., 2017b),
86 and in Yedoma regions of Alaska and Siberia (Murton et al., 2017). Thaw slumps are widespread
87 throughout glaciated terrain in the western Canadian Arctic (Kokelj et al., 2017b; Lantuit et al. 2012),
88 including on the Peel Plateau (Lacelle et al., 2015). These dynamic landforms develop via the ablation of
89 an ice-rich headwall and are particularly efficient at thawing thick zones of ice-rich permafrost and
90 translocating large volumes of sediment from slopes to downstream environments (see Fig. 1). RTS
91 features remain active for decades (Lantuit et al. 2012). They typically stabilize following sediment
92 accumulation at the base of the headwall (Kokelj et al., 2015), but can reactivate causing thaw within
93 the scar zone and upslope expansion of the disturbance (Kokelj et al., 2013; Lantuit and Pollard, 2008).
94 During periods of activity, thawed materials accumulate as a saturated slurry in the slump scar zone (see
95 Fig. 1b) and are transported downslope by mass flow processes, which are accelerated by meltwater-
96 and rainfall-induced saturation (Kokelj et al. 2015). Surface runoff can also remove solutes and
97 suspended sediment from the thawed substrate to downstream environments. Although variation in
98 temperature, precipitation and solar radiation have been correlated with development rates and growth
99 of RTS features (Kokelj et al., 2009, 2013, 2015; Lacelle et al., 2010; Lewkowicz, 1986, 1987), we know
100 little about how these and other environmental drivers might control permafrost-DOC dynamics at the
101 individual-slump to small watershed scale.

102 On the Peel Plateau, an individual thaw slump can impact tens of hectares of terrain, displace
103 hundreds of thousands of cubic meters of sediments, and significantly alter surface water sediment and
104 solute loads (Kokelj et al., 2013; Malone et al., 2013), and thus downstream ecosystems (Chin et al.,
105 2016; Malone et al., 2013). The magnitude of these disturbances and their cumulative impacts is great
106 enough to alter solute loads in the Peel River (70,000 km² watershed area; Kokelj et al., 2013), even

Deleted: ; Kokelj and Jorgenson, 2013

Deleted: ,

Deleted: – through the coupling of geomorphic and thermal processes –

Deleted: ,

Deleted: translocated

Deleted: During active and stabilized periods, s

114 though only a small portion of that river's total catchment area (<1%) is influenced by thermokarst
115 (Kokelj et al., 2017b; Segal et al., 2016). This contrasts with many other thaw-affected regions, where
116 increases in solute loads following permafrost disturbance can be transient, and have little overall effect
117 on annual solute fluxes (e.g., in High Arctic regions affected by active layer detachments; Lafrenière &
118 Lamoureux, 2013). In addition, permafrost thaw on the Peel Plateau is notable in that it exposes vast
119 quantities of mineral-rich glacial till, which is overlain by a relatively shallow layer of slightly more
120 organic-rich soils (Duk-Rodkin and Hughes, 1992; Kokelj et al. 2017a). Although this till-associated, RTS-
121 susceptible landscape type is found across the Laurentide and Barents-Kara glacial margins of Canada,
122 Alaska, and Siberia (Kokelj et al. 2017b), it contrasts with regions of Alaska and eastern Siberia that are
123 either Yedoma-rich or were covered by patchy or thin drift during the late Pleistocene, and have been a
124 focus for study of permafrost-DOC interactions to date (Abbott et al., 2014, 2015; Drake et al., 2015;
125 Mann et al., 2012; Vonk et al., 2013b).

Deleted: (e.g., limited to spring freshet)

Deleted: for example

Deleted: patchily glaciated

Deleted: which

Deleted: common

Deleted: points

126 Thermokarst has been documented to enhance DOC concentrations in recipient aquatic
127 ecosystems in several Arctic regions (Frey and McClelland, 2009; Tank et al., 2012a; Vonk et al., 2013a;
128 Vonk and Gustafsson, 2013). In Alaska, streams affected by thaw slumps have higher DOC
129 concentrations than un-affected systems across various terrain types (2-3 fold increase; Abbot et al.,
130 2014), while in eastern Siberia the DOC concentration in runoff from thawing Yedoma is considerably
131 greater than concentrations in recipient river systems (~30-fold elevation; Spencer et al. 2015).
132 However, multiple factors, including variable carbon content in permafrost soils (Hugelis et al. 2014) and
133 variation in ground ice type and volume (Fritz et al. 2015) may affect DOC release from permafrost. In
134 regions where thermokarst transports fine-grained sediments to aquatic systems, sorption processes
135 may also be important, because dissolved organic matter (DOM) can readily sorb to mineral soils (e.g.,
136 Kothawala et al. 2009). Sorption to mineral sediments can cause DOM to be rapidly removed from
137 solution in stream systems (Kaiser and Guggenberger, 2000; Kothawala et al. 2009; McDowell, 1985),
138 while enabling the downstream transport and continued sequestration of organic carbon (Hedges et al.,

Deleted: draining

Deleted: also

147 1997). This process may be particularly important for regulating DOC dynamics in glacial margin
148 landscapes, where a predisposition to thaw slumping results in an abundance of thermokarst-related
149 slope disturbances which mobilize fine-grained glacial sediment stores to downstream systems (Kokelj
150 et al., 2017a, 2017b; Lantuit et al. 2012; Rampton, 1988). Despite this, we know little about the
151 downstream consequences of permafrost thaw for carbon biogeochemistry in till-dominated glacial
152 landscapes, which are emerging as some of the most geomorphically dynamic permafrost environments
153 in the circumpolar Arctic,
154 The objective of this study was to quantify how RTS features affect the concentration and
155 composition of DOC across a series of slump-affected streams on the Peel Plateau, and to examine how
156 observed variation in slump morphometry affects DOC dynamics in downstream environments. We
157 further investigated how short-term variation in precipitation, temperature, and solar radiation affect
158 DOC delivery from land to water, using measurements of DOC flux above and below a single RTS feature.
159 We targeted the thermokarst-sensitive Peel Plateau for this work, which is characteristic of till-rich,
160 glacial margin landscapes throughout Canada, Alaska, and Siberia (Kokelj et al. 2017b). By comparing our
161 results to those from elsewhere, we highlight how broad variation in permafrost soil composition,
162 permafrost genesis, and Quaternary history may drive variation in land-freshwater DOC dynamics across
163 divergent regions of the warming circumpolar Arctic,

Deleted: such as those in the western Canadian Arctic

Deleted: Although the mechanisms governing the thaw-mediated transport of DOC from land to freshwater seem likely to differ in till-dominated landscapes when compared to other regions studied to date

Deleted: is known

Deleted: regions

Deleted: such as the Peel Plateau

Deleted: is

Deleted: slump-affected

Deleted: other regions

Deleted: this allows us to consider

Deleted: affected by permafrost thaw

166 2 Study Site

167 2.1 General study site description

168 Our study was conducted on the Peel Plateau, situated in the eastern foothills of the Richardson
169 Mountains, NWT, Canada, in the zone of continuous permafrost (Fig. 1a). The fluvially-incised Plateau
170 ranges in elevation from 100 to 650 masl. The region was covered by the Laurentide Ice Sheet (LIS) for a
171 brief period (a maximum of 2,000-3,000 years) 18,500 cal yr BP (Lacelle et al., 2013). The bedrock of the

185 region is Lower Cretaceous marine shale from the Arctic River formation (Norris, 1984) and siltstone
 186 overlain by Late Pleistocene glacial, glacio-fluvial and glacio-lacustrine sediments (Duk-Rodkin and
 187 Hughes, 1992). These Pleistocene deposits host ice-rich permafrost, overlain by a shallow and commonly
 188 organic-rich active layer. Radiocarbon dating in the region has placed the age of relict ground ice in the
 189 late Pleistocene ($18,100 \pm 60$ ¹⁴Cyr BP; Lacelle et al., 2013). Upper layers of permafrost thawed during
 190 the early Holocene and host younger, Holocene-aged organic materials (Lacelle et al., 2013). These are
 191 distinguished from deeper Pleistocene-aged permafrost by a thaw unconformity (Burn 1997; Fig. 1),
 192 which developed when warmer climate during the early Holocene prompted the thawing of near-
 193 surface permafrost. The regional increase in active layer thickness integrated organic matter into the
 194 thawed soils and enabling the leaching of soluble ions (see Fig. 1c-d). Climate cooling and permafrost
 195 aggradation have archived this notable stratigraphic variation in geochemistry, organic matter content,
 196 and cryostructure (Burn 1997; Fritz et al. 2012; Kokelj et al., 2002; Lacelle et al., 2014; Murton and
 197 French, 1994).

198 Ice-marginal glaciogenic landscapes such as the Peel Plateau host thick layers of ice-rich
 199 sediments, and thus have a predisposed sensitivity to climate-driven thaw slump activity (Kokelj et al.,
 200 2017). On the Peel Plateau, slumping is largely constrained by the maximum extent of the LIS, because
 201 the thick layers of ice-rich permafrost necessary for RTS activity are typically not present beyond the
 202 glacial limits (Lacelle et al., 2015). Fluvial incision provides the topographic gradient necessary for thaw
 203 slump development and RTS features are common; ranging in size from numerous small features, to
 204 those greater than 20 ha, which are rare (<5% prevalence; Lacelle et al., 2015). The recent intensification
 205 of slumping on the Peel Plateau is driven in part by increasing air temperatures and summer rainfall
 206 intensity (Kokelj et al., 2015). This intensification is also increasing the thaw of the deepest layer of ice-
 207 rich, organic-poor, Pleistocene-aged glaciogenic tills that underlie this region. The pattern of abundant
 208 thaw slump development across ice-marginal glaciated permafrost landscapes extends from the Peel
 209 Plateau across the western Canadian Arctic, and persists at continental scales (Kokelj et al., 2017b).

Deleted: , covered by a shallow organic layer

Deleted: epoch

Deleted: 7890 ± 250 ¹⁴Cyr BP;

Deleted: clearly delineated

Deleted: and a

Deleted: ,

Deleted: and integration of organic matter into these previously thawed soils

Deleted: Subsequent

Deleted: of permafrost due to gradual cooling

Deleted: s

Deleted: its

Deleted: , newly developing

Deleted: which are relatively numerous,

224

225 2.2 Regional climate

226 The regional climate is typical of the subarctic with long, cold winters and short, cool summers.
227 Mean annual air temperature (1981-2010) at the Fort McPherson weather station (Fig. 1a) is -7.3 °C
228 with average summer (June-August) temperatures of 13.3 °C (Environment Canada, 2015). A warming
229 trend of 0.77 °C per decade since 1970 has been recorded; however these increases are most apparent
230 in the winter months (Burn and Kokelj, 2009). Our sample period spanned the thaw months of July and
231 August; average 1981-2010 temperatures for those months, recorded at Fort McPherson, are 15.2 and
232 11.8 °C, respectively, similar to temperatures at Fort McPherson during 2014 (15.6 and 11.6 °C), but
233 slightly higher than 2014 averages observed at a recently established meteorological station on the Peel
234 Plateau (Fig. 1a; 13.2 °C in July and 9.5 °C in August). Annual cumulative rainfall (1981-2010) at Fort
235 McPherson averages 145.9 mm, with July and August having the highest rainfall levels at 46.4 and 39.1
236 mm (Environment Canada, 2015). In 2014, rainfall for July and August was 71 and 121 mm at Fort
237 McPherson, and 128.7 and 170.7 mm on the Peel Plateau. This continues the trend for this region of
238 increasingly wet summers with numerous extreme rainfall events (Kokelj et al., 2015).

239

240 3 Methods

241 3.1 Slump site selection

242 Eight RTS features were selected from across the study region, using aerial surveys and previous
243 knowledge of the region (Fig. 1; Fig. S1; Table 1). Selected slumps were characterized by a debris tongue
244 that connected the slump to the valley bottom and directly impacted a stream system. Sampling at each
245 slump occurred at three discrete locations: upstream, within-slump, and downstream of slump influence
246 (Fig. 1b). Upstream sites were trunk streams that connected with the slump flow path further
247 downstream, and were un-affected by any major geomorphic disturbance and thus representative of an
248 undisturbed, pristine environment. Within-slump sampling occurred at points of channelized slump

Deleted: features across this landscape

Deleted: possessed

Deleted: extended to

Deleted: locations were locations of

253 runoff within the scar zone or upper debris tongue. Downstream sampling locations were below the
254 confluence of the sampled upstream flow and all within-slump runoff paths, and were chosen to be
255 representative of slump impact on aquatic ecosystems across the Peel Plateau landscape. In one
256 instance (Slump HD, August 17), a fluidized flow event between sampling events saturated the scar zone
257 and obliterated within-slump channelized surface flow. As a result, the within-slump sample taken at
258 this site was not representative of typical channelized slump runoff that characterized all other slump
259 sampling conditions, and has been discarded from all analyses.

Deleted: located

260 A general classification of the slumps is difficult as these features are influenced by a diverse
261 range of geomorphic processes that vary in intensity over time (Table 1; Fig. S1). Three of the slumps
262 (FM4, FM2, FM3) are classified as 'mega slumps', characterised by areas greater than 5 ha, a headwall
263 greater than 4 m in height, and a debris tongue that connects the slope to the valley below (Kokelj et al.,
264 2013, 2015). Of these, FM4 possesses a headwall approximately 20 m in height, but was largely
265 stabilized in 2014 (Fig. S1). FM2 is among the largest active slumps in the region, with a headwall 25-30

Deleted: ,

266 m high and visible as a much smaller feature in air photos since 1944 (Lacelle et al. 2015). Slump FM3,
267 which was the focus for 'environmental controls' work (further described below), covers an area of
268 approximately 10 ha with a headwall of approximately 10 m height and a debris tongue that extends
269 nearly 600 m down valley (Table 1). Headwall retreat rate at FM3 over a 20 year period has been
270 calculated at 12.5 m yr⁻¹ (Lacelle et al., 2015). FM2 and FM3 geochemistry and geomorphology were
271 previously described by Malone et al. (2013). SD is the smallest and youngest slump that we studied,

Deleted: indicated by the small outflow, long, dry, and significantly revegetated debris tongue

Moved down [1]: FM2 geochemistry and geomorphology were previously described by Malone et al. (2013).

Deleted: chosen

Deleted: our

Deleted: , and has

Deleted: in

Moved (insertion) [1]

272 and was initiated when diversion of a small creek caused lateral bank erosion. In 2014, the SD headwall
273 was 2-4 m high with no defined debris tongue and a scar zone extending approximately 20m upslope,

Deleted: , and no defined debris tongue

274 The remaining slump sites (HA, HB, HC, HD) were all well-developed active RTS features with headwalls
275 similar to, or smaller than, FM3, but with smaller debris tongues (Table 1). With the exception of SD,
276 slump headwalls exposed permafrost well below a thaw unconformity, indicating that Pleistocene-aged,
277 unweathered glacial materials were being thawed (Lacelle et al., 2013).

Deleted: much smaller in volume

Deleted: by the slump

291

292 *3.2 Field sampling and data collection*

293 *3.2.1 The effect of slumping on DOC and stream water chemistry*

294 The majority of our sampling was conducted during the summer of 2014. Of the eight slumps
295 that were sampled, three were accessed from the Dempster Highway three times over the sampling
296 season, one (FM3; see also Sect. 3.2.2) was accessed twice from the highway, and four were accessed
297 twice via helicopter (Table 1). At each of the upstream, downstream, and within-slump sampling
298 locations, specific conductivity, pH, and temperature were recorded using a YSI Pro Plus multi-
299 parameter meter. Water samples were collected from directly below the stream surface into 1 L acid
300 washed HDPE bottles and allowed to sit in chilled, dark conditions for 24 h to enable the considerable
301 sediments in these samples to partially settle out of suspension. Sample water was then filtered with
302 pre-combusted (475 °C, 4 hours) Whatman GF/F filters (0.7 µm pore size). Filtered sample water was
303 transferred into 40 mL acid washed, pre-combusted glass bottles for DOC analysis, or 60 mL acid washed
304 HDPE bottles for the analysis of absorbance and major ions. DOC samples were acidified with
305 hydrochloric acid (1 µL mL⁻¹), following Vonk et al. (2015b). The GF/F filters were retained for analysis of
306 total suspended solids (TSS). Samples for stable water isotopes were collected directly from streams into
307 acid washed 40 mL HDPE bottles with no headspace and sealed. During summer 2016, samples were
308 additionally collected from a subset of slump locations (FM2, FM3, FM4 and SD) for the ¹⁴C signature of
309 DOC at upstream and within-slump sites. DO¹⁴C samples were collected in acid-washed polycarbonate
310 bottles, allowed to settle for 24 h, and filtered using pre-combusted Whatman GF/F filters into pre-
311 combusted glass media bottles with phenolic screw caps and butyl septa. All samples were refrigerated
312 until analysis. Absorbance samples were analyzed within 1 week of collection, cation samples within 4
313 months of collection, and DOC (including ¹⁴C) samples within 1-2 months of collection. Samples for Fe
314 and δ¹⁸O were analyzed within 6 months of collection.

315

Deleted: with

317 3.2.2 Environmental controls on DOC flux

318 To explore how environmental variables control the flux of DOC from RTS-affected streams, we
319 visited slump FM3 an additional 17 times beyond the sampling described above. This intensively-studied
320 site was chosen to be representative of active Peel Plateau slumps that are eroding Holocene- to
321 Pleistocene-aged sediments. During each visit, we measured discharge at the upstream and downstream
322 locations to calculate DOC flux, and collected upstream and downstream DOC concentration samples.
323 Downstream discharge was measured using an OTT C2 current meter at three locations across the small
324 stream and at 40 % depth. Due to the shallow, low flow conditions at the upstream site, upstream
325 discharge was measured using the cross sectional method (Ward and Robinson, 2000). In both cases,
326 discharge was calculated as the product of velocity and stream cross-sectional area. Local daily climate
327 data were obtained from an automated meteorological station established in 2010 by the Government
328 of the Northwest Territories (Kokelj et al. 2015). The station is located within 2 km of slump FM3 (Fig.
329 1a) and is instrumented for the measurement of air temperature, rainfall, and net radiation.

330

331 3.3 Laboratory analyses

332 3.3.1 Major ions, dissolved organic carbon, $\delta^{18}\text{O}$ and DO^{14}C

333 Cation concentrations (Ca^{2+} , Mg^{2+} , Na^+) were analyzed on a Perkin Elmer Analyst 200 Atomic
334 Absorption Spectrometer at York University. A subset of collected samples were analyzed for total
335 dissolved Fe at the University of Alberta on an Inductively Coupled Plasma - Optical Emission
336 Spectrometer (Thermo Scientific ICP6300), to allow for the correction of our Specific UV Absorbance
337 results (see below). DOC samples were analyzed on a Shimadzu TOC-V analyzer; DOC was calculated as
338 the mean of the best 3 of 5 injections with a coefficient of variation of <2%; the precision of a 10 mg L⁻¹
339 caffeine standard across all sample runs was 0.32 mg L⁻¹. A Picarro liquid water isotope analyzer was
340 used to measure $\delta^{18}\text{O}$ at the University of Alberta, following filtration (0.45 μm cellulose acetate,
341 Sartorius) into 2 mL autosampler vials (National Scientific), without headspace. The precision of our

342 $\delta^{18}\text{O}$ analysis is $\pm 0.2\%$. The radiocarbon signature of DOC was measured following extraction and
343 purification at the A.E. Lalonde AMS facility (University of Toronto) using a 3MV tandem accelerator
344 mass spectrometer (High Voltage Engineering) following established methodologies (Lang et al., 2016;
345 Palstra and Meijer, 2014; Zhou et al., 2015), and is reported with an error estimate of 1σ .

346

347 3.3.2 Total suspended solids

348 Samples for TSS were filtered in the field for later analysis, ensuring that there was enough
349 sediment on the pre-combusted (475 °C, 4 hours) and pre-weighed GF/F filters. Filters were stored
350 frozen, dried at 60 °C for 8 hours, placed in a desiccator overnight and promptly weighed. TSS was
351 calculated as the difference in filter weight before and after sediment loading, divided by volume
352 filtered.

353

354 3.3.3 Dissolved organic matter spectral characteristics

355 DOM composition was assessed using absorbance-based metrics. A 5 cm quartz cuvette was
356 used to obtain UV-visible spectra data from 250-750 nm, using a Genesys 10 UV-Vis spectrophotometer.
357 A baseline correction was applied to eliminate any minor interference from particles $< 0.7\ \mu\text{m}$ (Green
358 and Blough 1994). Specific UV absorbance at 254 nm (SUVA_{254}), which is correlated with DOM
359 aromaticity (Weishaar and Aiken, 2003), was calculated by dividing the decadal absorbance at 254 nm
360 (m^{-1}) by the DOC concentration (mg L^{-1}). SUVA_{254} values were corrected for Fe interference following
361 Poulin et al. (2014) using maximum Fe concentrations from laboratory analyses or as reported in Malone
362 et al. (2013). Spectral slopes between 275 and 295 nm, and 350 and 400 nm ($S_{275-295}$, $S_{350-400}$) were
363 calculated following Helms et al. (2008), and are reported as positive values to adhere to mathematical
364 conventions. Slope ratios (S_R), which correlate with DOM molecular weight (Helms et al., 2008), were
365 calculated as the ratio of $S_{275-295}$ to $S_{350-400}$.

366

367 *3.4 Statistical analyses and calculations*

368 Statistical analyses were completed in R version 3.1.3 (R Core Team, 2015) using packages 'nlme'
369 (Pinheiro et al., 2015), 'lme4' (Zeileis and Hothorn, 2002), 'lmerTest' (Curtin, 2015), 'car' (Fox and
370 Weisberg, 2011), and 'zoo' (Zeileis and Grothendieck, 2005). The effect of slumping on stream chemistry
371 and optical characteristics was assessed using linear mixed effects models in the 'nlme' package of R. For
372 each parameter, analyses were split into two separate models that included data for upstream and
373 downstream chemistry, and upstream and within-slump chemistry. We used this approach to separately
374 assess the effects of slumping downstream of slump systems, and to compare the composition of slump
375 runoff to nearby, pristine environments. For each analysis, we included slump location (see Table 1) as a
376 random effect, and considered models that either nested Julian date within the random effect of slump
377 location, or allowed Julian date to occur as a fixed effect. The best model was chosen using the Akaike
378 Information Criterion (AIC), and best-fit models were refit with a variance structure to ensure that
379 model assumptions were met. The variance structures varIdent (for within-slump site and slump
380 location) and varFixed (for Julian date) were used together (using varComb) and in isolation for this
381 purpose (Zuur et al., 2009). AIC values for the weighted and un-weighted models were again compared
382 to choose a final model of best fit for each analysis.

383 We used the high-frequency data from slump FM3 to assess how environmental conditions
384 (rainfall, temperature, solar radiation) and TSS affect DOC delivery to slump-affected streams. To do
385 this, we conducted multiple linear regressions, using AIC values to determine models of best fit
386 (Burnham and Anderson, 2002). To enable a specific assessment of environmental controls on
387 downstream DOC flux, upstream DOC flux was separated out into a distinct regression analysis, because
388 upstream DOC flux was strongly correlated with flux downstream, and therefore overwhelmed all
389 environmental variables in the downstream model. Models were tested for serial correlation using the
390 auto-correlation function, and models with variance inflation factors greater than 10 or significant
391 Durbin Watson test results (indicative of correlated variables; Durbin & Watson, 1950; Hair et al., 1995)

392 were discarded. Residuals were examined to ensure the model was a good fit for the data (Zuur et al.,
393 2009). We considered both time-of-sampling (0 h) and past (48, 72, and 120 h) environmental conditions
394 in our analyses. Because cumulative values for environmental variables (i.e. accumulated rainfall in the
395 previous 48, 72 and 120 h) showed a strong positive correlation to one another, we used temporally
396 shifted data (i.e. rainfall 48, 72 and 120 h prior to the DOC flux measurement) in the final model. Similar
397 models were also constructed to examine the effects of environmental drivers on DOC concentration.
398 Differences in paired upstream-downstream measures of DOC flux and concentration at slump FM3
399 were also assessed using a Wilcoxon Signed Rank Test, a non-parametric analog to the paired-t test.

400 Following our finding of decreasing DOC concentrations downstream of slumps (see Sect. 4.1
401 and 5.1) we used data from slump FM3, where we have upstream, downstream, and within-slump DOC
402 concentration measurements, and upstream and downstream discharge measurements, to calculate a
403 mass balance for DOC across the three sampling locations. These data – available for all three locations
404 on two dates during the summer of 2014 – were used to calculate DOC flux at upstream and
405 downstream sites as $\text{flux}_{\text{DOCdown}} = [\text{DOC}]_{\text{down}} \cdot \text{discharge}_{\text{down}}$ or $\text{flux}_{\text{DOCup}} = [\text{DOC}]_{\text{up}} \cdot \text{discharge}_{\text{up}}$, and at
406 within-slump sites as $\text{flux}_{\text{DOCwithin}} = [\text{DOC}]_{\text{within}} \cdot (\text{discharge}_{\text{down}} - \text{discharge}_{\text{up}})$. We calculate a similar mass
407 balance for TSS, which we use as a rough tracer for the inflow of slump runoff over the < 1 km span
408 between upstream and downstream locations at this site.

409

410 **4. Results**

411 *4.1 DOC concentration across slump sites*

412 While DOC concentrations ranged broadly across pristine streams on the Peel Plateau (Fig. 2;
413 from 5.4 to 26.1 mg L⁻¹ at upstream, pristine sites), concentrations consistently declined downstream of
414 slumps, when compared to paired, upstream locations ($p < 0.001$; Fig. 2; Table 2). Although this effect
415 was modest (typically less than 20 %; Fig. 2), it occurred reliably across all slump sites. In contrast,
416 comparisons of upstream and within-slump sites showed no consistent trend in DOC concentration,

417 when evaluated across all slump locations ($p=0.153$; Fig. 2; Table 2). Instead, the effects of slumping on
418 the DOC concentration of slump runoff varied by site. At the largest, most well-developed slump
419 complexes (FM4, FM2, and FM3), where debris tongues are extensive and thaw extends well into the
420 deepest layer of Pleistocene-aged glacial materials, DOC concentrations tended to be lower in slump
421 runoff than at the paired upstream sites (Fig. 2). At more modestly-sized slumps (HB, HC, and HD),
422 where modern and relict Holocene active layers comprise a greater proportion of thawed materials,
423 within-slump DOC concentrations tended to be higher than values upstream (Fig. 2). Within each site,
424 DOC concentrations were relatively consistent across the 2-3 sampling periods (Fig. 2).

Deleted: sites

Deleted: the

Deleted: s form

Deleted: the actively thawing headwal

Deleted: l

425

426 4.2 Bulk chemistry of pristine waters and slump runoff

427 To better understand how the input of slump runoff affects downstream DOC, we examined
428 concentrations of major ions, conductivity and TSS as ‘tracers’ of slump activity, because these
429 constituents have previously been shown to be significantly affected by slumping in this region (Kokelj et
430 al., 2005, 2013; Malone et al., 2013; Thompson et al., 2008). Major ion (Ca^{2+} , Mg^{2+} , Na^+) concentrations
431 in slump runoff were considerably greater than in pristine streams (a 2.7 to 11.7-fold increase; Fig. 3b-d;
432 Table 2). These patterns were similar, though muted, at slump-affected downstream sites, where major
433 ion concentrations were 1.5 to 3.5-fold greater than at pristine sites (Fig. 3b-d; Table 2). Mean
434 conductivity also increased significantly as a result of slumping ($p < 0.001$; Table 2): within-slump sites
435 had conductivity values that were 9.2-fold greater than upstream sites, while downstream values were
436 an average of 2.6 times greater than those upstream (Fig. 3e). Finally, TSS was also significantly elevated
437 at slump-affected sites ($p < 0.001$; Table 2) with concentrations being more than two orders of
438 magnitude greater within slumps, and more than one order of magnitude greater downstream, when
439 compared to upstream sites (Fig. 3a). The effect of slump runoff on downstream chemistry is also
440 reflected in DOC: ion, and DOC: TSS ratios, which decreased markedly between upstream and
441 downstream locations. For example, molar ratios of ($\text{Ca}^{2+} + \text{Mg}^{2+}$): DOC averaged 0.78 ± 0.37 (mean \pm

Deleted: Average

Deleted: levels

Deleted: when compared to upstream

450 standard error) upstream of slumps, but 2.07 ± 0.45 downstream, while average gram-weight ratios of
451 TSS: DOC were 32 ± 12 upstream, but 1454 ± 332 at downstream locations.

452

453 4.3 Spectral and isotopic characteristics

454 SUVA₂₅₄, which is positively correlated with DOM aromaticity (Weishaar and Aiken, 2003), was
455 significantly lower within slumps, and downstream of slumps, than in upstream, pristine, environments
456 ($p < 0.001$; Fig. 4; Table 2). Mean within-slump SUVA₂₅₄ was less than half of that observed for pristine
457 waters (Fig. 4), while downstream values declined by approximately 20 %. In accordance with the
458 SUVA₂₅₄ results, $S_{275-295}$, $S_{350-400}$, and S_R were all significantly greater within slumps when compared to
459 upstream sites ($p < 0.001$; Fig. 4; Table 2), indicating lower DOM molecular weight within slumps (Helms
460 et al., 2008). Differences in slope parameters between upstream and downstream locations were muted
461 relative to the within-slump: upstream comparisons (Fig. 4), with $S_{275-295}$ ($p = 0.011$) and S_R ($p < 0.001$)
462 increasing significantly, but more modestly, downstream of slumps, and $S_{350-400}$ declining slightly
463 ($p = 0.001$; Fig. 4; Table 2).

464 Upstream $\delta^{18}O$ averaged $-20.1 \text{‰} \pm 0.12$, which corresponds to a modern active-layer pore
465 water $\delta^{18}O$ signature for this region (Lacelle et al., 2013; Fig. 5). Within-slump $\delta^{18}O$ was discernibly
466 depleted when compared to upstream locations, with mean values of $-22.7 \text{‰} \pm 0.72$, which falls
467 between previously-identified regional endmembers for Pleistocene-aged ground ice ($18,100 \pm 60 \text{ }^{14}\text{Cyr}$
468 BP) and the modern active layer (Lacelle et al., 2013; Fig. 5). Within-slump $\delta^{18}O$ was also much more
469 variable between RTS features than upstream and downstream $\delta^{18}O$ values. Similar to upstream sites,
470 downstream $\delta^{18}O$ clustered near the modern active layer $\delta^{18}O$ endmember, but with a small depletion
471 that was consistent with a contribution from slump inflow ($-20.7 \text{‰} \pm 0.21$).

472 To further investigate the effect of water source on DOM composition, we examined the
473 relationship between SUVA₂₅₄ and $\delta^{18}O$. More depleted samples taken from within-slump sites had
474 clearly depressed SUVA₂₅₄ values when compared to samples with more enriched $\delta^{18}O$ (Fig. 5). Of the

Deleted: Average

Deleted: active

Deleted: average

478 large, most well-developed slumps that were identified in Sect. 4.1, two (FM2 and FM3), in addition to
479 site HB, had $\delta^{18}\text{O}$ values that were more depleted than the Holocene-aged icy diamicton values reported
480 in Lacelle et al. (2013), suggesting some contribution of runoff from older, Pleistocene-aged permafrost
481 (Fig. 5). It is likely that the $\delta^{18}\text{O}$ signal at the relatively stable mega-slump site (FM4) was somewhat
482 diluted by the 7.2 mm of rainfall that fell in the 48 hours preceding our sample. Although sites FM3 and
483 SD received 12.4 and 3.5 mm of rain, respectively, in the 48 hours prior to sampling, these are both
484 much more active slump sites, and thus less prone to dilution of the slump outwash signature. There
485 was no significant rainfall immediately preceding sampling at any other sites.

486 The radiocarbon signature of DOC from upstream and within-slump locations at sites FM4, FM2,
487 FM3, and SD largely mirrors the $\delta^{18}\text{O}$ results. DOC from sites upstream of slump disturbance was
488 approximately modern in origin (ranging from 217 ± 24 ^{14}C yr BP to modern in age; Table 3). In contrast,
489 within-slump waters from site FM2 and FM3 were early Holocene-aged (9592 ± 64 , and 8167 ± 39 ^{14}C yr
490 BP, respectively; Table 3). Slump runoff from site SD was older than at upstream sites, but younger than
491 for the larger slumps, described above (1157 ± 23 ^{14}C yr BP; Table 3).

492

493 4.4 Patterns and environmental drivers of DOC flux

494 Similar to our findings for the distributed sampling scheme (Fig. 2), downstream DOC
495 concentration was consistently lower than concentrations upstream, across the 19 paired
496 measurements taken at the intensively studied site FM3 ($p < 0.001$, $N=19$, $W=0$; Wilcoxon Signed Rank
497 Test; mean decline of 2.5 ± 0.2 mg L^{-1} , compared to a mean upstream concentration of 13.6 ± 0.5 mg L^{-1}).
498 To explore environmental drivers of DOC movement within this landscape, however, we focus on
499 DOC flux, which allows a direct assessment of slump-mediated DOC addition to this system.
500 Downstream DOC flux (mg s^{-1}) tended to be slightly greater than upstream flux on most, but not all,
501 sampling occasions (Fig. 6). As a result, paired comparisons indicate no statistical difference between
502 upstream and downstream DOC flux at this site (Wilcoxon signed rank test; $p=0.096$, $N=19$, $W=53$).

Deleted: s

Deleted: slump

Deleted: slump FM3;

506 Because upstream and downstream DOC flux were strongly correlated to one another ($r^2 = 0.94$;
507 $p < 0.0001$), our downstream model was run without upstream DOC flux as a predictor variable. The best-
508 fit multiple linear regression model for downstream DOC flux ($r^2 = 0.84$; $p < 0.01$) retained seven
509 variables, of which two were significant (Table 4). Of these, air temperature (72 h prior to sampling)
510 showed a negative relationship with downstream DOC flux while rainfall (0 h; time of sampling) showed
511 a strong positive relationship (Table 4). The best-fit model for upstream DOC flux ($r^2 = 0.87$; $p < 0.001$)
512 also retained seven variables, of which four were significant ($p < 0.05$; Table 4). Similar to the
513 downstream analysis, air temperature (0 h, 72 h) displayed a negative relationship, and time-of-
514 sampling (0 h) rainfall a strong positive relationship, with DOC flux (Table 4). However, 120 h rainfall
515 showed a negative relationship with DOC flux in this model. Regressions assessing controls on
516 downstream DOC flux relative to upstream flux (i.e., as a ratio, or the difference between the two
517 values) were not significant. Models to explore controls on upstream and downstream DOC
518 concentration were also relatively similar to one another, showing strong, positive relationships
519 between DOC concentration and air temperature, and more modest negative relationships between
520 DOC concentration and net radiation (Table 4).

521

522

523 5. Discussion

524 5.1 Retrogressive thaw slumps and carbon delivery to streams of the Peel Plateau

525 In both Eastern Siberia (Spencer et al. 2015; Vonk et al., 2013b) and Alaska (Abbott et al., 2014)
526 permafrost slumping has been associated with significant increases in DOC mobilization from terrestrial
527 to aquatic systems. Our data show that this was not the case on the Peel Plateau, where the landscape-
528 induced variation in DOC concentration among pristine stream sites was much greater than the change
529 in stream water DOC as a result of slumping. Across all of our study sites, DOC concentrations
530 consistently declined downstream of slumps when compared to upstream locations, while at an

Deleted: had

Deleted: had

Deleted: permafrost thaw features

Deleted: decreased

535 intensively-sampled slump, DOC flux did not differ significantly between upstream and downstream
536 locations. In contrast, comparisons of channelized slump runoff (our within-slump sites) and paired un-
537 affected sites showed no consistent DOC trend. Instead, DOC concentrations in slump runoff were either
538 greater than, or less than, their comparison upstream locations, in a manner that differed depending on
539 slump morphological characteristics such as slump size and headwall height (Fig. 1; see further
540 discussion in Sect. 5.3). The moderate effect of slumping on DOC concentration occurred despite the
541 significant influence of these disturbances on the delivery of many biogeochemical constituents to
542 recipient streams. For example, conductivity was approximately one order of magnitude greater, and
543 TSS two orders of magnitude greater, in slump-derived runoff than at upstream, un-affected sites. This
544 led to substantially increased TSS:DOC and (Ca + Mg):DOC ratios downstream of slumps, when
545 compared to pristine, upstream locations.

546 Decreasing DOC concentrations downstream of slumps, despite increasing concentrations of
547 indicators of slump activity (major ions, TSS) could be driven by several, potentially co-occurring
548 mechanisms. In some locations, decreases may be partially caused by low DOC concentrations in slump
549 outflow (a dilution effect; see slumps FM2, FM3, and FM4 in Fig. 2; further discussed in Sect. 5.3).
550 However, our results suggest that DOC sorption to suspended inorganic sediments could also play a role
551 in regulating DOC dynamics in slump-affected systems. At multiple sites (HB, HC, and HD), DOC
552 concentrations declined downstream of slumps despite a modest elevation in DOC concentration in
553 slump drainage waters (Fig. 2). Thermokarst contributes significant amounts of fine-grained glacial
554 sediment to fluvial systems on the Peel Plateau (Kokelj et al., 2013; silty-clay sediment classification for
555 FM3 in Lacelle et al., 2013). DOC sorption can occur in seconds to minutes in freshwater systems (Qualls
556 and Haines, 1992), with fine-grained materials being particularly conducive to this process (Kothawala et
557 al., 2009). Data from site FM3, where we have upstream and downstream discharge data coupled with
558 DOC and TSS concentrations at upstream, downstream, and within-slump locations on two separate
559 dates, allows possible DOC sorption to be assessed. On these dates, DOC flux declined downstream of

Deleted: result from

Deleted: on the Peel Plateau

Deleted: us to assess

Deleted: at this site

Deleted: declines

565 the slump (i.e., $\text{flux}_{\text{DOCdown}} < \text{flux}_{\text{DOCup}}$), despite a clear and measurable efflux of DOC from the slump to
566 the receiving stream system ($\text{flux}_{\text{DOCwithin}}$; Fig. 7). This same calculation using TSS as a rough tracer of
567 slump inflow shows the calculated efflux of TSS from this slump ($\text{flux}_{\text{TSSwithin}}$) to be almost identical to the
568 increase in TSS flux downstream of the disturbance (as $\text{flux}_{\text{TSSdown}} - \text{flux}_{\text{TSSup}}$; Fig. 7). Thus, it seems likely
569 that relatively rapid processes, such as sorption to mineral surfaces, are affecting DOC dynamics in
570 thermokarst-affected fluvial systems on the Peel Plateau.

Deleted: downstream

571 Although a similar decrease in DOC concentration with slumping has been found for lakes in this
572 region (Kokelj et al., 2005), our findings contrast with those from other previously-studied areas of the
573 Arctic, where thermokarst leads to an efflux of high-DOC waters from slump features (e.g., Abbott et al.,
574 2014; Vonk et al., 2013a). However, ice-marginal glaciated landscapes are common throughout the
575 western Canadian Arctic, and in many other Arctic regions. The thick, mineral-rich, carbon-poor tills with
576 high ice contents that characterize these landscapes is predisposed to intense thaw slumping and the
577 mobilization of glacial sediments from slope to stream (Kokelj et al., 2017b). As a result, DOC
578 'sequestration' following slumping seems unlikely to be limited to the Peel Plateau. Given the high TSS
579 export and apparent organic carbon sorption to glacial sediments observed with slumping on the
580 Peel Plateau, we expect that substantial organic carbon is mobilized from these disturbances in the
581 particle-attached, rather than dissolved, form (i.e., as particulate organic carbon; POC). Quantifying this
582 POC mobilization and fate once subject to contemporary biogeochemical processing, and the
583 mechanisms that enable DOC sequestration to occur, are key avenues for future research on the Peel
584 Plateau and elsewhere.

Deleted: work to-date in

Deleted: has been demonstrated to

Deleted: I

Deleted: however,

Deleted: This terrain type is characterized by

Deleted: but

Deleted: , and

Deleted: are

Deleted: climate-driven

Deleted: release

Deleted: slumps

Deleted: , its

Deleted: ,

585

586 5.2 The effect of retrogressive thaw slumps on DOM composition

587 Although DOC concentrations did not increase in RTS-affected streams, absorbance metrics
588 clearly indicate that slump-derived DOM on the Peel Plateau is compositionally different than DOM from
589 upstream locations. Upstream waters had significantly higher SUVA_{254} values than downstream and

Deleted: Despite the fact that

605 within-slump sites (Table 2, Fig. 4). Similarly, while the average S_R of Peel Plateau upstream waters (0.74
606 ± 0.005) was within the range of S_R typically associated with fresh, terrestrial DOM (~ 0.70 ; Helms et al.,
607 2008), values were significantly greater within-slump (0.92 ± 0.015) and downstream (0.89 ± 0.009)
608 (Table 2, Fig. 4), indicating decreasing DOM molecular weight as a result of RTS activity. High $SUVA_{254}$
609 values accompanied by low S_R at upstream sites suggest that water flow in undisturbed catchments is
610 restricted to shallow, organic-rich flowpaths through the active layer, with permafrost inhibiting water
611 contributions from deeper, groundwater or mineral-associated sources (Balcarczyk et al., 2009;
612 MacLean et al., 1999; Mann et al., 2012; O'Donnell et al., 2010; Street et al. 2016). In contrast, within-
613 slump and downstream measurements indicate a clear transition in DOM source.

614 The comparatively low $SUVA_{254}$, and high S_R values for downstream and within-slump sites
615 indicate that permafrost-derived carbon on the Peel Plateau is characterized by relatively low molecular
616 weight and aromaticity, and is thus similar in its composition to permafrost carbon from other regions.
617 For example, $SUVA_{254}$ values were low in waters draining active thaw slumps when compared to
618 stabilized and undisturbed sites on the North Slope of Alaska (Abbott et al., 2014), while in Siberia, ^{14}C -
619 depleted DOM from small tributary streams affected by thermokarst had lower $SUVA_{254}$ values
620 compared to younger DOM from the Kolyma River mainstem (Mann et al., 2015; Neff et al., 2006).
621 Although $SUVA_{254}$ values for waters draining Peel Plateau thaw slumps are slightly lower than those
622 reported for Siberian Yedoma disturbances (Mann et al., 2015), the overall similarity of permafrost-
623 derived DOM composition across these various regions is striking, given the regional differences in
624 permafrost origin and landscape history. For example, ~~the~~ DOM released by permafrost thaw on the
625 Peel Plateau is till-associated, and early-Holocene in mean age, while east Siberian Yedoma is composed
626 of loess-derived Pleistocene deposits that sequestered carbon in association with synengetic permafrost
627 aggradation. This suggests that common processes may enable the organic matter contained in
628 permafrost soils to become compositionally similar across diverse Arctic regions. Such compositional
629 similarity also indicates that permafrost-origin DOM from the Peel Plateau – similar to that from other

Deleted: depositional

Deleted: while

Deleted: of permafrost

633 regions (Abbott et al., 2014; Drake et al., 2015) – may be readily degraded by bacteria, despite the
634 divergent origin of this carbon.

635

636 5.3 The effect of slump morphometry on runoff water biogeochemistry

637 $\delta^{18}\text{O}$ and DO^{14}C data provide further evidence that intense slumping enables novel sources of
638 water and solutes to be transported to fluvial systems on the Peel Plateau. For most of the RTS features
639 that we studied, the $\delta^{18}\text{O}$ signature of within-slump waters ranged from similar to the 'icy diamicton'
640 that overlies the early Holocene thaw unconformity, to that for underlying Pleistocene-aged ground ice
641 (Lacelle et al., 2013; Fig. 5). Similarly, DO^{14}C from a subset of sites indicates slump-derived DOC is early
642 Holocene in age for all but the shallowest slump surveyed. This suggests that our slump outflow samples
643 were likely comprised of a mixture of Pleistocene-, Holocene-, and modern-sourced water (see Fig. 1c-
644 e), but that the contribution of these end-members varied across slumps depending on the relative
645 volume of different stratigraphic units being mobilized.

646 The between-site variation in $\delta^{18}\text{O}$ signature (Fig. 5) and relative DOC concentration (Fig. 2b) of
647 slump runoff waters appears to be related to differences in slump morphometry (size, headwall height,
648 and the length and area of the debris tongue; see Table 1 and Fig. 1c-e) across sites. The well-developed,
649 larger slump complexes (FM4, FM2 and FM3) were more likely to have $\delta^{18}\text{O}$ signatures that lie between
650 end-member values for Holocene-aged icy diamicton and Pleistocene-aged ground ice (Fig. 5; although
651 note that dry and stabilized FM4 differs somewhat from this trend). These well-developed slumps also
652 stood out as displaying within-slump DOC concentrations that were lower than at upstream comparison
653 sites (Fig. 2b). The headwall exposure at these largest slumps exposes Pleistocene-aged permafrost to
654 several m depth (see Fig. 1c), while the evacuation of scar zone materials have produced extensive
655 debris tongues up to several km long (Table 1, Figs. 1b, S1e and S1g). This significant exposure of
656 mineral-rich, Pleistocene-aged glacial till contributes solutes from low-carbon mineral soils and low-DOC
657 ground ice (Fritz et al. 2015; Tanskii et al. 2016) to runoff, while entraining fine-grained sediments which

Deleted: those

Deleted: those

660 provide mineral surface area for possible DOC adsorption. Adsorption may be further enhanced as
661 slump and stream runoff continue to entrain sediments as flows incise the lengthy debris tongue
662 deposits. In contrast, slumps with slightly shallower headwalls (HA, HB, HC, HD; see Fig. 1d), and less
663 well-developed debris tongues (Table 1), appear to elicit a slightly different response than the largest
664 slumps discussed above. At these mid-sized sites, within-slump DOC concentrations were typically
665 higher than those found at upstream comparison sites (Fig. 2b), which may reflect the greater relative
666 inputs from thawing of the Holocene-aged relict active layer, and decreased interaction with debris
667 tongue deposits at these smaller disturbances. Similarly, runoff $\delta^{18}\text{O}$ tends to lie between Holocene and
668 modern end-member values at these sites (though note the more depleted value for HB; Fig. 5),
669 indicating a lower relative contribution of Pleistocene-aged ground ice to slump outflow waters.

670 Finally, the youngest and shallowest slump surveyed (SD), exposed only near-surface permafrost
671 soils for leaching and geochemical transport (Figs. 1e and S1; Table 1), and not the underlying mineral
672 and ice-rich glacial substrates. Accordingly, the effects of slumping on stream chemistry, optical
673 parameters, and isotopes were muted at SD when compared to the larger slumps discussed above.
674 These morphometry-related shifts in the downstream effects of slumping suggest that we should expect
675 non-linearity in the biogeochemical response as RTS features develop over time, particularly if slumping
676 continues to intensify with future warming on the Peel Plateau (e.g., Kokelj et al., 2017b), underscoring
677 the importance of long-term monitoring on the Peel Plateau and elsewhere.

679 5.4 Environmental controls on DOC flux and concentration

680 Air temperature and rainfall exerted the strongest control on DOC flux at our intensively studied
681 site, which was chosen to be representative of active Peel Plateau slumps that eroding Holocene- to
682 Pleistocene-aged sediments (slump FM3; Fig. 6; Table 4). Upstream of the slump, rainfall was positively
683 correlated, and air temperature negatively correlated, with DOC flux. However, precipitation events
684 were negatively related to temperature (Fig. 6), suggesting that over a single season, precipitation

Deleted: exposes

Deleted: appear

Deleted:).

Deleted: This

Deleted: es

Deleted: , and indicates that the incorporation of non-linearity into modelling efforts is critical for predicting future change

Deleted: are

Deleted: are

Deleted: at the upstream site

Deleted: at the single-season scale of our investigation

697 served as the primary environmental control on upstream DOC flux. DOC concentration was relatively
 698 constant with upstream discharge ($r=-0.342$, $p=0.151$), indicating that precipitation controlled DOC flux
 699 largely as a result of changes in runoff, and that DOC was not source-limited over the time scale of our
 700 investigation. However, upstream DOC concentration was positively related to temperature (Table 4),
 701 suggesting a link between biological activity and within-soil DOC production (c.f. Pumpanen et al., 2014).
 702 These upstream-of-slump results are consistent with work from other undisturbed permafrost and
 703 boreal regions, where precipitation and catchment runoff have been shown to control DOC flux in
 704 streams (Prokushkin et al., 2005; Pumpanen et al., 2014), and increasing temperature has been shown
 705 to increase DOC production in soils (Christ and David, 1996; Neff and Hooper, 2002; Prokushkin et al.,
 706 2005; Yanagihara et al., 2000). They are also consistent with the concept that the permafrost barrier
 707 forces runoff to travel through the shallow active layer, where high hydraulic conductivity leads to rapid
 708 transport of carbon into fluvial systems (O'Donnell et al., 2010; Striegl et al., 2005).
 709 Slumping did not significantly affect downstream DOC flux at the intensively studied slump site,
 710 when compared to DOC flux upstream (Fig. 6; Sect. 4.4). Although concentration consistently declined
 711 downstream at FM3 (Sect. 4.1 and 4.4), downstream DOC flux was either slightly higher, or slightly
 712 lower, than upstream flux; a result that seems likely to play out at other, comparable Peel Plateau
 713 slumps, given the coherent concentration patterns that we observed across this landscape. Concordant
 714 with the lack of slump effect on DOC flux, neither the ratio of (downstream: upstream) or difference
 715 between (downstream – upstream) upstream and downstream DOC flux could be explained by any of
 716 our environmental variables, while the environmental controls on downstream flux were almost
 717 identical to those upstream (Table 4). The lack of clear environmental control on relative downstream:
 718 upstream DOC flux occurred despite the fact that precipitation has been shown to be a strong driver of
 719 sediment movement from slump features on the Peel Plateau, at time scales similar to those used for
 720 this work (Kokelj et al., 2015).

Deleted: upstream

Deleted: controls

Deleted: water flow in pristine streams on the Peel Plateau

Deleted: that

Deleted: is an important regulator of

Deleted: precipitation

Deleted: ,

Deleted: and little degradation in soils

Deleted: of this site

Deleted: with slumping

Deleted: change in

Deleted: in response to slumping

Deleted: downstream flux showed an almost identical relationship with environmental controls as those upstream

Deleted: ablation and

721 Considering the Peel Plateau landscape as a whole, it appears that precipitation serves as a

737 primary, positive control on DOC flux. Thus, this study adds DOC production to the list of changes – such
738 as increasing slump activity and sediment mobilization – that can be expected with the increased
739 precipitation that is affecting this region, and is predicted for many Arctic locations (IPCC, 2014; Kokelj et
740 al., 2015). However, it appears that slumping does not over-ride the landscape-scale control on DOC flux
741 in this system – at least at the scale of this single-season – perhaps because processes like DOC sorption
742 mask the influx of slump-derived DOC (Fig. 6). This result highlights the complexity of the interaction
743 between changing climatic parameters and DOC dynamics on the Peel Plateau, where thaw slumps of
744 increasing size mobilize till, glaciolacustrine, glaciofluvial, and organic deposits, while also draining
745 contemporary active layers across a shrub-tundra to spruce forest upland gradient. DOC dynamics are
746 thus affected by both water and carbon generation across these variable landform types, and by
747 biogeochemical interactions such as mineral adsorption in recipient systems. Future work to tease apart
748 the interactions between changing climatic parameters, slump development, and resultant
749 biogeochemical effects is clearly warranted, with the recognition that environmental controls on slump
750 activity, and thus downstream biogeochemistry, can be expected to show marked regional variation (see
751 for example, work from Eureka Sound; Grom & Pollard 2008).

Deleted: increases in

Deleted: are underway in

Deleted: are

Deleted: regions

Deleted: slump features

Deleted: incorporate thawing

Deleted: While f

Deleted: on the Peel Plateau and elsewhere, we must also recognize

753 6. Conclusions: Dissolved carbon mobilization across diverse permafrost landscapes

Deleted: 5.5

Deleted: Study implications and future research directions

754 Carbon dynamics in Arctic aquatic systems are influenced by numerous factors, including
755 geology, Quaternary and glacial history, soil composition, vegetation, active layer dynamics, and the
756 nature and intensity of thermokarst. As a result, the effect of permafrost thaw on DOC concentration
757 and flux should – at a fundamental level – vary across broad, regional scales. Our results demonstrate
758 that we can expect marked inter-regional variation in DOC transport to streams in response to
759 permafrost degradation. For example, declines in DOC concentration downstream of slumps on the Peel
760 Plateau clearly differ from what has been found in eastern Siberia and regions of Alaska, where
761 thermokarst releases substantial quantities of DOC (e.g., Spencer et al. 2015), and increases DOC

774 concentrations in downstream systems (Abbott et al. 2015). Efforts that incorporate information
775 concerning the geology and Quaternary history of thawing landscapes, the physical and geochemical
776 composition of permafrost soils, and the nature and intensity of thermokarst processes within
777 landscapes (see, for example, Olefeldt et al. 2016) will considerably increase our ability to predict
778 climate-driven changes in carbon delivery from land to water on a pan-Arctic scale.

779 At finer scales, this work underscores the variability of thermokarst effects within regions, and
780 the local-scale control on this variability. On the Peel Plateau, between-site differences in the
781 biogeochemical effect of thermokarst are related to variation in soil stratigraphy (i.e., the relative depth
782 of the Holocene-aged paleo-active layer) and ever-evolving slump morphometry. Although striking
783 within-region variability in biogeochemical response to thermokarst has been seen elsewhere (e.g.,
784 Watanabe et al., 2011), responses in other regions occur as a result of very different – and region-
785 specific – landscape-level drivers. This landscape-specificity also extends to the non-linear

786 biogeochemical response as thermokarst features develop over time. Changes in downstream
787 biogeochemistry with slump development are very different on the Peel Plateau, for example, than in
788 other regions (e.g., Abbot et al. 2015), while temporal non-linearity can also be expected for other types
789 of permafrost thaw (Kokelj et al. 2002, Vonk et al. 2016), such as increasing active layer thickness
790 (Romanovsky et al. 2010). It seems clear that a tiered approach, targeted within regions to understand
791 local controls on thaw-driven DOC mobilization, and across regions to document the effects of broad-
792 scale variation imposed by geological and climate legacy, is required to understand future
793 biogeochemical functioning of thermokarst-affected landscapes in a warming circumpolar Arctic.

Deleted: accurately

Deleted: how

Deleted: will respond to climate change

Deleted: however,

Deleted: for example,

Deleted: correspond

Deleted: slump

Deleted:),

Deleted: while n

Deleted: to extend to

Deleted: different

Deleted: ,

Deleted: Only with a

Deleted: where we work

Deleted: how

Deleted: drive regional responses to thaw

Deleted: how

Deleted: predictable, broad-scale variation controls responses at continental to pan-Arctic scales

Deleted: will we be able to

Deleted:

Deleted: the

Deleted: throughout Arctic regions

819 **Data availability:** Data associated with this manuscript have been made available in Tables S1 and S2.

820

821 **Competing interests:** The authors declare that they have no conflict of interest.

822

823 **Acknowledgements**

824 Financial support for this research was provided by Ontario Graduate Scholarship, York University
825 Fieldwork Cost Fund, York University Research Cost Fund, Northern Scientific Training Program, NSERC
826 Discovery and Northern Research Supplement grants to SET, the Campus Alberta Innovates Program,
827 and the Polar Continental Shelf Program. We would like to thank Scott Zolkos for his support as a field
828 assistant and for the production of Figure 1; S. Tetlich, D. Neyando, and P. Snowshoe for field sampling
829 assistance; and the Tetlit Gwich'in (Fort McPherson) Renewable Resources Council. Sarah Shakil and
830 Scott Zolkos assisted with the collection of samples for DO¹⁴C; Justin Kokoszka performed geospatial
831 calculations of slump area and debris tongue length. Comments from Michael Fritz and one anonymous
832 reviewer greatly improved the content of the manuscript. NWT Geological Survey contribution number

833 xxxx.

834

Deleted:

836 **Literature Cited**

- 837 Abbott, B. W., Larouche, J. R., Jones, J. B., Bowden, W. B., and Balsler, A. W.: Elevated dissolved organic
838 carbon biodegradability from thawing and collapsing permafrost, *J. Geophys. Res.*, 119, 2049–2063,
839 doi:10.1002/2014JG002678, 2014.
- 840 Abbott, B. W., Jones, J. B., Godsey, S. E., Larouche, J. R., and Bowden, W. B.: Patterns and persistence of
841 hydrologic carbon and nutrient export from collapsing upland permafrost, *Biogeosciences*, 12,
842 3725–3740, doi:10.5194/bg-12-3725-2015, 2015.
- 843 Balcarczyk, K. L., Jones, J. B., Jaffé, R., and Maie, N.: Stream dissolved organic matter bioavailability and
844 composition in watersheds underlain with discontinuous permafrost, *Biogeochemistry*, 94, 255–270,
845 doi:10.1007/s10533-009-9324-x, 2009.
- 846 Battin, T. J., Kaplan, L. A., Findlay, S., Hopkinson, C. S., Marti, E., Packman, A. I., Newbold, J. D., and
847 Sabater, F.: Biophysical controls on organic carbon fluxes in fluvial networks, *Nat. Geosci.*, 1, 95–100,
848 doi:10.1038/ngeo101, 2008.
- 849 Burn, C. R.: Cryostratigraphy, paleogeography, and climate change during the early Holocene warm
850 interval, western Arctic coast, Canada. *Can. J. Earth Sci.* 34, 912-925, doi: 10.1139/e17-076, 1997.
- 851 Burn, C. R. and Kokelj, S. V.: The environment and permafrost of the Mackenzie Delta area, *Permafr.*
852 *Periglac. Process.*, 20, 83–105, doi:10.1002/ppp.655, 2009.
- 853 Burnham, K. P. and Anderson, D. R.: *Model Selection and Multi- Model Inference: A Practical*
854 *Information-Theoretic Approach*, Springer, New York., 2002.
- 855 Chin, K. S., Lento, J., Culp, J. M., Lacelle, D., and Kokelj, S. V.: Permafrost thaw and intense thermokarst
856 activity decreases abundance of stream benthic macroinvertebrates, *Glob. Chang. Biol.*, 22, 2715–
857 2728, doi:10.1111/gcb.13225, 2016.
- 858 Christ, M. J. and David, M. B.: Temperature and moisture effects on the production of dissolved organic
859 carbon in a Spodosol, *Soil Biol. Biochem.*, 28, 1191–1199, doi:10.1016/0038-0717(96)00120-4, 1996.
- 860 Curtin, J.: *lmSupport: Support for Linear Models*. R package version 2.9.2., 2015.
- 861 Dittmar, T. and Kattner, G.: The biogeochemistry of the river and shelf ecosystem of the Arctic Ocean: a
862 review, *Mar. Chem.*, 83, 103–120, doi:10.1016/S0304-4203(03)00105-1, 2003.
- 863 Drake, T. W., Wickland, K. P., Spencer, R. G. M., McKnight, D. M., and Striegl, R. G.: Ancient low-
864 molecular-weight organic acids in permafrost fuel rapid carbon dioxide production upon thaw, *Proc.*
865 *Natl. Acad. Sci.*, 112, 13946–13951, doi:10.1073/pnas.1511705112, 2015.
- 866 Duk-Rodkin, A. and Hughes, O. L.: *Surficial Geology, Fort McPherson-Bell River, Yukon-Northwest*
867 *Territories*. Geological Survey of Canada, Map 1745A, scale 1:250 000, Geological Survey of Canada,
868 Map 1745A, scale 1:250 000, 1992.
- 869 Durbin, J. and Watson, G. S.: Testing for serial correlation in least squares regression I, *Biometrika*, 37,
870 409–428, 1950.

- 871 Environment Canada: Canadian Climate Normals 1981-2010 Station Data, Fort McPherson, 2015.
- 872 Fox, J. and Weisberg, S.: An {R} Companion to Applied Regression, Second Edition. Thousand Oaks CA:
873 Sage. <http://socserv.socsci.mcmaster.ca/jfox/Books/Companion.>, 2011.
- 874 Frey, K. E. and McClelland, J. W.: Impacts of permafrost degradation on arctic river biogeochemistry,
875 *Hydrol. Process.*, 23, 169–182, doi:10.1002/hyp, 2009.
- 876 Fritz, M., Vonk, J. E., and Lantuit, H.: Disappearing Arctic coastlines, *Nat. Clim. Change*, 7, 6-7,
877 doi:10.1038/nclimate3188, 2017.
- 878 Fritz, M., Opel, T., Tanski, G., Herzsuh, U., Meyer, H., Eulenbug, A., and Lantuit, H.: Dissolved organic
879 carbon (DOC) in Arctic ground ice, *The Cryosphere*, 9, 737-752, doi:10.5194/tc-9-737-2015, 2015.
- 880 Fritz, M., Wetterich, S., Schirrmeister, L., Meyer, H., Lantuit, H., Preusser, F., and Pollard, W. H.: Eastern
881 Beringia and beyond: Late Wisconsinan and Holocene landscape dynamics along the Yukon Coastal
882 Plain, Canada. *Palaeogeogr. Palaeoclimatol. Palaeoecol.*, 319–320, 28–45, doi:
883 10.1016/j.palaeo.2011.12.015, 2012.
- 884 Fulton, R. J.: *Surficial Materials of Canada*, Natural Resources Canada., 1995.
- 885 Green, S. A. and Blough, N. V.: Optical absorption and fluorescence properties of chromophoric
886 dissolved organic matter in natural waters, *Limnol. Oceanogr.*, 39, 1903–1916,
887 doi:10.4319/lo.1994.39.8.1903, 1994.
- 888 Hair, J. F. J., Anderson, R. E., Tatham, R. L., and Black, W. C.: *Multivariate Data Analysis*, 3rd ed.,
889 Macmillan, New York., 1995.
- 890 Hedges, J. I., Keil, R. G., and Benner, R.: What happens to terrestrial organic matter in the ocean?, *Org.*
891 *Geochem.*, 27, 195–212, 1997.
- 892 Helms, J. R., Stubbins, A., Ritchie, J. D., Minor, E. C., Kieber, D. J., and Mopper, K.: Absorption spectral
893 slopes and slope ratios as indicators of molecular weight, source, and photobleaching of
894 chromophoric dissolved organic matter, *Limnol. Oceanogr.*, 53, 955–969,
895 doi:10.4319/lo.2008.53.3.0955, 2008.
- 896 Holmes, R. M., McClelland, J. W., Peterson, B. J., Tank, S. E., Bulygina, E., Eglinton, T. I., Gordeev, V. V.,
897 Gurtovaya, T. Y., Raymond, P. A., Repeta, D. J., Staples, R., Striegl, R. G., Zhulidov, A. V., and Zimov, S.
898 A.: Seasonal and annual fluxes of nutrients and organic matter from large rivers to the Arctic Ocean
899 and surrounding seas, *Estuaries and Coasts*, 35, 369–382, doi:10.1007/s12237-011-9386-6, 2012.
- 900 Hugelius, G., Strauss, J., Zubrzycki, S., Harden, J. W., Schuur, E. A. G., Ping, C. L., Schirrmeister, L., Grosse,
901 G., Michaelson, G. J., Koven, C. D., O'Donnell, J. A., Elberling, B., Mishra, U., Camill, P., Yu, Z.,
902 Palmtag, J., and Kuhry, P.: Estimated stocks of circumpolar permafrost carbon with quantified
903 uncertainty ranges and identified data gaps, *Biogeosciences*, 11, 6573–6593, doi:10.5194/bg-11-
904 6573-2014, 2014.
- 905 IPCC: Topic 2: Future Climate Changes, Risks, and Impacts In *Climate Change 2014: Synthesis Report.*
906 *Contribution of Working Groups I, II and III to the Fifth Assessment Report of the Intergovernmental*
907 *Panel on Climate Change [Core Writing Team, R.K. Pachauri and L.A. Meyer (eds.)]. IPCC, Geneva,*

- 908 Switzerland, 151 pp, Geneva, Switzerland., 2014.
- 909 Kaiser, K. and Guggenberger, G.: The role of DOM sorption to mineral surfaces in the preservation of
910 organic matter in soils, *Org. Geochem.*, 31, 711–725, doi:10.1016/S0146-6380(00)00046-2, 2000.
- 911 Khvorostyanov, D. V., Krinner, G., Ciais, P., Heimann, M., and Zimov, S. A.: Vulnerability of permafrost
912 carbon to global warming. Part I: Model description and role of heat generated by organic matter
913 decomposition, *Tellus, Ser. B Chem. Phys. Meteorol.*, 60 B, 250–264, doi:10.1111/j.1600-
914 0889.2007.00333.x, 2008a.
- 915 Khvorostyanov, D. V., Ciais, P., Krinner, G., Zimov, S. A., Corradi, C., and Guggenberger, G.: Vulnerability
916 of permafrost carbon to global warming. Part II: Sensitivity of permafrost carbon stock to global
917 warming, *Tellus, Ser. B Chem. Phys. Meteorol.*, 60 B, 265–275, doi:10.1111/j.1600-
918 0889.2007.00336.x, 2008b.
- 919 Kokelj, S. V., Tunnicliffe, J. F., and Lacelle, D.: The Peel Plateau of northwestern Canada : an ice-rich
920 hummocky moraine landscape in transition, in *Landscapes and Landforms of western Canada*,
921 edited by O. Slaymaker, pp. 109–122, Springer International Publishing, Switzerland., 2017a.
- 922 Kokelj, S. V. and Jorgenson, M. T.: Advances in thermokarst research, *Permafr. Periglac. Process.*, 24,
923 108–119, doi:10.1002/ppp.1779, 2013.
- 924 Kokelj, S. V., Smith, C. A., and Burn, C. R.: Physical and chemical characteristics of the active layer and
925 permafrost, Herschel Island, western Arctic Coast, Canada, *Permafr. Periglac. Process.*, 13, 171–185,
926 doi:10.1002/ppp.417, 2002.
- 927 Kokelj, S. V., Jenkins, R. E., Milburn, D., Burn, C. R., and Snow, N.: The influence of thermokarst
928 disturbance on the water quality of small upland lakes, Mackenzie Delta region, Northwest
929 Territories, Canada, *Permafr. Periglac. Process.*, 16, 343–353, doi:10.1002/ppp.536, 2005.
- 930 Kokelj, S. V., Lantz, T. C., Kanigan, J. C., Smith, S. L., and Coutts, R.: Origin and polycyclic behaviour of
931 tundra thaw slumps, Mackenzie Delta region, Northwest Territories, Canada, *Permafr. Periglac.*
932 *Process.*, 20, 173–184, doi:10.1002/ppp, 2009.
- 933 Kokelj, S. V., Lacelle, D., Lantz, T. C., Tunnicliffe, J., Malone, L., Clark, I. D., and Chin, K. S.: Thawing of
934 massive ground ice in mega slumps drives increases in stream sediment and solute flux across a
935 range of watershed scales, *J. Geophys. Res. Earth Surf.*, 118, 681–692, doi:10.1002/jgrf.20063, 2013.
- 936 Kokelj, S. V., Tunnicliffe, J., Lacelle, D., Lantz, T. C., Chin, K. S., and Fraser, R.: Increased precipitation
937 drives mega slump development and destabilization of ice-rich permafrost terrain, northwestern
938 Canada, *Glob. Planet. Change*, 129, 56–68, doi:10.1016/j.gloplacha.2015.02.008, 2015.
- 939 Kokelj, S. V., Lantz, T. C., Tunnicliffe, J., Segal, R., and Lacelle, D.: Climate-driven thaw of permafrost
940 preserved glacial landscapes, northwestern Canada, *Geology*, 45, 371–374, doi:10.1130/G38626.1,
941 2017b.
- 942 Kothawala, D. N., Moore, T. R., and Hendershot, W. H.: Soil properties controlling the adsorption of
943 dissolved organic carbon to mineral soils, *Soil Sci. Soc. Am. J.*, 73, 1831–1842,
944 doi:10.2136/sssaj2008.0254, 2009.

945 Lacelle, D., Bjornson, J., and Lauriol, B.: Climatic and geomorphic factors affecting contemporary (1950-
946 2004) activity of retrogressive thaw slumps on the Aklavik Plateau, Richardson Mountains, NWT,
947 Canada, *Permafr. Periglac. Process.*, 21, 1–15, doi:10.1002/ppp.666, 2010.

948 Lacelle, D., Lauriol, B., Zazula, G., Ghaleb, B., Utting, N., and Clark, I. D.: Timing of advance and basal
949 condition of the Laurentide Ice Sheet during the last glacial maximum in the Richardson Mountains,
950 NWT, *Quat. Res. (United States)*, 80, 274–283, doi:10.1016/j.yqres.2013.06.001, 2013.

951 Lacelle, D., Fontaine, M., Forest, A. P., and Kokelj, S.: High-resolution stable water isotopes as tracers of
952 thaw unconformities in permafrost: A case study from western Arctic Canada, *Chem. Geol.*, 368, 85–
953 96, doi:10.1016/j.chemgeo.2014.01.005, 2014.

954 Lacelle, D., Brooker, A., Fraser, R. H., and Kokelj, S. V.: Distribution and growth of thaw slumps in the
955 Richardson Mountains–Peel Plateau region, northwestern Canada, *Geomorphology*, 235, 40–51,
956 doi:10.1016/j.geomorph.2015.01.024, 2015.

957 Lafrenière, M. J. and Lamoureux, S. F.: Thermal perturbation and rainfall runoff have greater impact on
958 seasonal solute loads than physical disturbance of the active layer, *Permafr. Periglac. Process.*, 24,
959 241–251, doi:10.1002/ppp.1784, 2013.

960 Lang, S. Q., McIntyre, C. P., Bernasconi, S. M., Früh-Green, G. L., Voss, B. M., Eglinton, T. I., and Wacker,
961 L.: Rapid ¹⁴C analysis of dissolved organic carbon in non-saline waters, *Radiocarbon*, 58, 505–515,
962 doi:10.1017/RDC.2016.17, 2016.

963 Lantuit, H. and Pollard, W. H.: Fifty years of coastal erosion and retrogressive thaw slump activity on
964 Herschel Island, southern Beaufort Sea, Yukon Territory, Canada, *Geomorphology*, 95, 84–102,
965 doi:10.1016/j.geomorph.2006.07.040, 2008.

966 Lantuit, H., Pollard, W. H., Couture, N., Fritz, M., Schirmermeister, L., Meyer, H., and Hubberten, H.W.:
967 Modern and late Holocene retrogressive thaw slump activity on the Yukon Coastal Plain and
968 Herschel Island, Yukon Territory, Canada. *Permafrost Periglacial Process.* 23, 39–51, doi:
969 10.1002/ppp.1731, 2012.

970 Lantz, T. C. and Kokelj, S. V.: Increasing rates of retrogressive thaw slump activity in the Mackenzie Delta
971 region, N.W.T., Canada, *Geophys. Res. Lett.*, 35, 1–5, doi:10.1029/2007GL032433, 2008.

972 Lewkowicz, A. G.: Rate of short-term ablation of exposed ground ice, Banks Island, Northwest
973 Territories, Canada, *J. Glaciol.*, 32, 511–519, 1986.

974 Lewkowicz, A. G.: Headwall retreat of ground-ice slumps, Banks Island, Northwest Territories, *Can. J.*
975 *Earth Sci.*, 24, 1077–1085, doi:10.1139/e87-105, 1987.

976 MacLean, R., Oswald, M. W., Irons, J. G., and McDowell, W. H.: The effect of permafrost on stream
977 biogeochemistry: A case study of two streams in the Alaskan (U.S.A.) taiga, *Biogeochemistry*, 47,
978 239–267, doi:10.1007/BF00992909, 1999.

979 Malone, L., Lacelle, D., Kokelj, S., and Clark, I. D.: Impacts of hillslope thaw slumps on the geochemistry
980 of permafrost catchments (Stony Creek watershed, NWT, Canada), *Chem. Geol.*, 356, 38–49,
981 doi:10.1016/j.chemgeo.2013.07.010, 2013.

- 982 Manley, W. F. and Kaufman, D. S.: Alaska PaleoGlacier Atlas: Institute of Arctic and Alpine Research
983 (INSTAAR), University of Colorado., 2002.
- 984 Mann, P. J., Davydova, A., Zimov, N., Spencer, R. G. M., Davydov, S., Bulygina, E., Zimov, S., and Holmes,
985 R. M.: Controls on the composition and lability of dissolved organic matter in Siberia's Kolyma River
986 basin, *J. Geophys. Res. Biogeosciences*, 117, G01028, doi:10.1029/2011JG001798, 2012.
- 987 Mann, P. J., Eglinton, T. I., McIntyre, C. P., Zimov, N., Davydova, A., Vonk, J. E., Holmes, R. M., and
988 Spencer, R. G. M.: Utilization of ancient permafrost carbon in headwaters of Arctic fluvial networks,
989 *Nat. Commun.*, 6, 7856, doi: 10.1038/ncomms8856, 2015.
- 990 McDowell, W. H.: Kinetics and mechanisms of dissolved organic carbon retention in a headwater stream,
991 *Biogeochemistry*, 1, 329–352, 1985.
- 992 Murton, J. and French, H.: Cryostructures in permafrost, Tuktoyaktuk coastlands, western arctic Canada,
993 *Can. J. Earth Sci.*, 31, 737–747, doi:10.1139/e94-067, 1994.
- 994 Murton, J. B., Edwards, M. E., Lozhkin, A. V., Anderson, P. M., Savvinov, G. N., Bakulina, N., Bondarenko,
995 O. V., Cherepanova, M. V., Danilov, P. P., Boeskorov, V., Goslar, T., Grigoriev, S., Gubin, S. V., Korzun, J.
996 A., Lupachev, A. V., Tikhonov, A., Tsygankova, V. I., Vasilieva, G. V., and Zanina, O. G.: Preliminary
997 paleoenvironmental analysis of permafrost deposits at Batagaika megaslump, Yana Uplands,
998 northeast Siberia, *Quat. Res.*, 87, 314–330, doi:10.1017/qua.2016.15, 2017.
- 999 Neff, J. C. and Hooper, D. U.: Vegetation and climate controls on potential CO₂, DOC and DON
1000 production in northern latitude soils, *Glob. Chang. Biol.*, 8, 872–884, doi:10.1046/j.1365-
1001 2486.2002.00517.x, 2002.
- 1002 Neff, J. C., Finlay, J. C., Zimov, S. A., Davydov, S. P., Carrasco, J. J., Schuur, E. A. G., and Davydova, A. I.:
1003 Seasonal changes in the age and structure of dissolved organic carbon in Siberian rivers and streams,
1004 *Geophys. Res. Lett.*, 33, 1–5, doi:10.1029/2006GL028222, 2006.
- 1005 Norris, D. K.: Geology of the northern Yukon and northwestern District of Mackenzie. Geological Survey
1006 of Canada, Map 1581A, scale 1:500 000, 1984.
- 1007 O'Donnell, J. A., Aiken, G. R., Kane, E. S., and Jones, J. B.: Source water controls on the character and
1008 origin of dissolved organic matter in streams of the Yukon River basin, Alaska, *J. Geophys. Res.*
1009 *Biogeosciences*, 115, 1–12, doi:10.1029/2009JG001153, 2010.
- 1010 Olefeldt, D., Goswami, S., Grosse, G., Hayes, D., Hugelius, G., Kuhry, P., McGuire, A. D., Romanovsky, V.
1011 E., Sannel, A. B. K., Schuur, E. A. G., and Turetsky, M. R.: Circumpolar distribution and carbon storage
1012 of thermokarst landscapes, 7, 13043, 2016.
- 1013 Palstra, S. and Meijer, H.: Biogenic carbon fraction of biogas and natural gas fuel mixtures determined
1014 with ¹⁴C, *Radiocarbon*, 56, 7–28, doi:10.2458/56.16514, 2014.
- 1015 Pinheiro, J., Bates, D., DebRoy, S., Sarkar, D., and R Core Team: nlme: Linear and nonlinear mixed effects
1016 models. R package version 3.1-120, <http://CRAN.R-project.org/package=nlme>., 2015.
- 1017 Poulin, B. A., Ryan, J. N., and Aiken, G. R.: Effects of iron on optical properties of dissolved organic
1018 matter, *Environ. Sci. Technol.*, 48, 10098–10106, doi:10.1021/es502670r, 2014.

- 1019 Prokushkin, A. S., Kajimoto, T., Prokushkin, S. G., McDowell, W. H., Abaimov, A. P., and Matsuura, Y.:
 1020 Climatic factors influencing fluxes of dissolved organic carbon from the forest floor in a continuous-
 1021 permafrost Siberian watershed, *Can. J. For. Res.*, 35, 2130–2140, doi:10.1139/x05-150, 2005.
- 1022 Pumpanen, J., A, L., Heli, M., Kolari, P., Ilvesniemi, H., Mammarella, I., Hari, O., Nikinmaa, E., Heinonsalo,
 1023 J., Back, J., Ojala, A., Berninger, F., and Vesala, T.: Precipitation and net ecosystem exchange are the
 1024 most important drivers of DOC flux in upland boreal catchments, *J. Geophys. Res. Biogeosciences*,
 1025 119, 1861–1878, doi:10.1002/2014JG002705, 2014.
- 1026 Qualls, R. and Haines, B. L.: Measuring adsorption isotherms using continuous, unsaturated flow through
 1027 intact soil cores, *Soil Sci. Soc. Am. J.*, 56, 456–460, doi:10.2136/sssaj1992.03615995005600020019x,
 1028 1992.
- 1029 R Core Team: R: A Language and Environment for Statistical Computing, R Foundation for Statistical
 1030 Computing, Vienna, Austria. <http://www.r-project.org/>, 2015.
- 1031 Rampton, V. N.: Quaternary geology of the Tuktoyaktuk coastlands, Northwest Territories, Geol. Surv.
 1032 Canada, 1988.
- 1033 Romanovsky, V. E., Smith, S. L., and Christiansen, H. H.: Permafrost thermal state in the polar Northern
 1034 Hemisphere during the international polar year 2007–2009: a synthesis, *Permafrost Periglacial*
 1035 *Process.*, 21, 106–116, doi: 10.1002/ppp.689, 2010.
- 1036 Schuur, E., Bockheim, J., Canadell, J. G., Euskirchen, E., Field, C. B., Goryachkin, S. V., Hagemann, S.,
 1037 Kuhry, P., Lafleur, P. M., Lee, H., Nelson, M. F. E., Rinke, A., Romanovsky, V. E., Shiklomanov, N.,
 1038 Tarnocai, C., Venevsky, S., Vogel, J. G., and Zimov, S. A.: Vulnerability of permafrost carbon to
 1039 climate change : Implications for the global carbon cycle, *Bioscience*, 58, 701–714,
 1040 doi:10.1641/B580807, 2008.
- 1041 Schuur, E. A. G., Abbott, B. W., Bowden, W. B., Brovkin, V., Camill, P., Canadell, J. G., Chanton, J. P.,
 1042 Chapin, F. S., Christensen, T. R., Ciais, P., Crosby, B. T., Czimczik, C. I., Grosse, G., Harden, J., Hayes, D.
 1043 J., Hugelius, G., Jastrow, J. D., Jones, J. B., Kleinen, T., Koven, C. D., Krinner, G., Kuhry, P., Lawrence,
 1044 D. M., McGuire, A. D., Natali, S. M., O’Donnell, J. A., Ping, C. L., Riley, W. J., Rinke, A., Romanovsky, V.
 1045 E., Sannel, A. B. K., Schädel, C., Schaefer, K., Sky, J., Subin, Z. M., Tarnocai, C., Turetsky, M. R.,
 1046 Waldrop, M. P., Walter Anthony, K. M., Wickland, K. P., Wilson, C. J., and Zimov, S. A.: Expert
 1047 assessment of vulnerability of permafrost carbon to climate change, *Clim. Change*, 119, 359–374,
 1048 doi:10.1007/s10584-013-0730-7, 2013.
- 1049 Schuur, E. A. G., McGuire, A. D., Grosse, G., Harden, J. W., Hayes, D. J., Hugelius, G., Koven, C. D., and
 1050 Kuhry, P.: Climate change and the permafrost carbon feedback, *Nature*, 520, 171–179,
 1051 doi:10.1038/nature14338, 2015.
- 1052 Segal, R. A., Lantz, T. C., and Kokelj, S. V.: Acceleration of thaw slump activity in glaciated landscapes of
 1053 the Western Canadian Arctic, *Environ. Res. Lett.*, 11, 34025, doi:10.1088/1748-9326/11/3/034025,
 1054 2016.
- 1055 Spencer, R. G. M., Mann, P. J., Dittmar, T., Eglinton, T. I., McIntyre, C., Holmes, R. M., Zimov, N., and
 1056 Stubbins, A.: Detecting the signature of permafrost thaw in Arctic rivers, *Geophys. Res. Lett.*, 42,
 1057 doi:10.1002/2015GL063498, doi:10.1002/2015GL063498, 2015.

1058 Street, L. E., Dean, J. F., Billett, M. F., Baxter, R., Dinsmore, K. J., Lessels, J. S., Subke, J.-A., Tetzlaff, D.,
1059 and Wookey, P. A.: Redox dynamics in the active layer of an Arctic headwater catchment; examining
1060 the potential for transfer of dissolved methane from soils to stream water, *J. Geophys. Res.*
1061 *Biogeosci.*, **121**, 2776-2792, doi: 10.1002/2016JG003387, 2016.

1062 Striegl, R. G., Aiken, G. R., Dornblaser, M. M., Raymond, P. A., and Wickland, K. P.: A decrease in
1063 discharge-normalized DOC export by the Yukon River during summer through autumn, *Geophys.*
1064 *Res. Lett.*, **32**, 1–4, doi:10.1029/2005GL024413, 2005.

1065 Tank, S. E., Raymond, P. A., Striegl, R. G., McClelland, J. W., Holmes, R. M., Fiske, G. J., and Peterson, B.
1066 J.: A land-to-ocean perspective on the magnitude, source and implication of DIC flux from major
1067 Arctic rivers to the Arctic Ocean, *Global Biogeochem. Cycles*, **26**, GB4018,
1068 doi:10.1029/2011GB004192, 2012a.

1069 Tank, S. E., Manizza, M., Holmes, R. M., McClelland, J. W., and Peterson, B. J.: The processing and impact
1070 of dissolved riverine nitrogen in the Arctic Ocean, *Estuaries and Coasts*, **35**, 401–415,
1071 doi:10.1007/s12237-011-9417-3, 2012b.

1072 Tanski, G., Couture, N., Lantuit, H., Eulenburg, A., and Fritz, M.: Eroding permafrost coasts release low
1073 amounts of dissolved organic carbon (DOC) from ground ice into the nearshore zone of the Arctic
1074 Ocean, *Glob. Biogeochem. Cycles*, **30**, 1054–1068, doi:10.1002/2015GB005337, 2016.

1075 Tanski, G., Lantuit, H., Ruttor, S., Knoblauch, C., Radosavljevic, B., Strauss, J., Wolter, J., Irrgang, A. M.,
1076 Ramage, J., and Fritz, M.: Transformation of terrestrial organic matter along thermokarst-affected
1077 permafrost coasts in the Arctic. *Sci. Total Environ.* 581–582, 434-447, doi:
1078 10.1016/j.scitotenv.2016.12.152, 2017.

1079 Thompson, M. S., Prowse, T. D., Kokelj, S. V., and Wrona, F. J.: The impact of sediments derived from
1080 thawing permafrost on tundra lake water chemistry: An experimental approach, *Proc. Ninth Int.*
1081 *Conf. Permafr.*, **29**, 1763–1768, 2008.

1082 Vonk, J. E. and Gustafsson, Ö.: Permafrost-carbon complexities, *Nat. Geosci.*, **6**, 675–676,
1083 doi:10.1038/ngeo1937, 2013.

1084 Vonk, J. E., Mann, P. J., Dowdy, K. L., Davydova, A., Davydov, S. P., Zimov, N., Spencer, R. G. M., Bulygina,
1085 E. B., Eglinton, T. I., and Holmes, R. M.: Dissolved organic carbon loss from Yedoma permafrost
1086 amplified by ice wedge thaw, *Environ. Res. Lett.*, **8**, 35023, doi:10.1088/1748-9326/8/3/035023,
1087 2013a.

1088 Vonk, J. E., Mann, P. J., Davydov, S., Davydova, A., Spencer, R. G. M., Schade, J., Sobczak, W. V., Zimov,
1089 N., Zimov, S., Bulygina, E., Eglinton, T. I., and Holmes, R. M.: High biolability of ancient permafrost
1090 carbon upon thaw, *Geophys. Res. Lett.*, **40**, 2689–2693, doi:10.1002/grl.50348, 2013b.

1091 Vonk, J. E., Tank, S. E., Mann, P. J., Spencer, R. G. M., Treat, C. C., Striegl, R. G., Abbott, B. W., and
1092 Wickland, K. P.: Biodegradability of dissolved organic carbon in permafrost soils and waterways: a
1093 meta-analysis, *Biogeosciences*, **12**, 6915–6930, doi:10.5194/bgd-12-8353-2015, 2015a.

1094 Vonk, J. E., Tank, S. E., Bowden, W. B., Laurion, I., Vincent, W. F., Alekseychik, P., Amyot, M., Billet, M. F.,
1095 Canário, J., Cory, R. M., Deshpande, B. N., Helbig, M., Jammot, M., Karlsson, J., Larouche, J.,
1096 Macmillan, G., Rautio, M., Walter Anthony, K. M., and Wickland, K. P.: Reviews and syntheses:

1097 Effects of permafrost thaw on Arctic aquatic ecosystems, *Biogeosciences*, 12, 7129–7167,
1098 doi:10.5194/bg-12-7129-2015, 2015b.

1099 Ward, R. C. and Robinson, M.: Principles of Hydrology, Fourth Edition, McGraw-Hill International (UK)
1100 Limited., 2000.

1101 Watanabe, S., Laurion, I., Chokmani, K., Pienitz, R., and Vincent, W. F.: Optical diversity of thaw ponds in
1102 discontinuous permafrost: A model system for water color analysis, *J. Geophys. Res. Biogeosciences*,
1103 116, doi:10.1029/2010JG001380, 2011.

1104 Weishaar, J. and Aiken, G.: Evaluation of specific ultra-violet absorbance as an indicator of the chemical
1105 content of dissolved organic carbon, *Environ. Chem.*, 37, 4702–4708, doi:10.1021/es030360x, 2003.

1106 Woods, G. C., Simpson, M. J., Pautler, B. G., Lamoureux, S. F., Lafrenière, M. J., and Simpson, A. J.:
1107 Evidence for the enhanced lability of dissolved organic matter following permafrost slope
1108 disturbance in the Canadian High Arctic, *Geochim. Cosmochim. Acta*, 75, 7226–7241,
1109 doi:10.1016/j.gca.2011.08.013, 2011.

1110 Yanagihara, Y., Koike, T., Matsuura, Y., Mori, S., Shibata, H., Satoh, F., Masuyagina, O., Zyryanova, O.,
1111 Prokushkin, A. S., Prokushkin, S. G., and Abaimov, A. P.: Soil respiration on the contrasting north-
1112 and south-facing slopes of a larch forests in Central Siberia, *Eurasian J. For. Res.*, 1, 19–29, 2000.

1113 Zeileis, A. and Grothendieck, G.: zoo: S3 infrastructure for regular and irregular time series, *J. Stat.*
1114 *Softw.*, 14, 1–27, 2005.

1115 Zeileis, A. and Hothorn, T.: Diagnostic checking in regression relationships., *R News*, 2, 7–10, 2002.

1116 Zhou, Y., Guo, H., Lu, H., Mao, R., Zheng, H., and Wang, J.: Analytical methods and application of stable
1117 isotopes in dissolved organic carbon and inorganic carbon in groundwater, *Rapid Commun. Mass*
1118 *Spectrom.*, 29, 1827–1835, doi:10.1002/rcm.7280, 2015.

1119 Zuur, A. F., Ieno, E. N., Walker, N., Saveliev, A. A., and Smith, G. M.: Mixed Effects Models and Extensions
1120 in Ecology with R, Springer, New York., 2009.

1121

1122

1123 **Table 1:** Slump characteristics and sampling information for eight retrogressive thaw slumps sampled
 1124 during the 2014 field season on the Peel Plateau, NWT, Canada. Characteristics are derived from
 1125 published values and field estimations.

Slump location	Sample dates (Julian day) ^a	Latitude	Longitude	Area (ha)	Debris tongue (m) ^b	Headwall height (m)
FM4	202, 210, 223	67 16.679	-135 09.573	8.8	960	16 to 20 ^d
FM2	200, 209, 222	67 15.462	-135 14.216	31.7	1529	25 ^e
FM3	197, 212	67 15.100	-135 16.270	6.1	576	10 ^e
SD	196, 213, 234	67 10.818	-135 43.630	3.3	NA	2 – 4 ^d
HA	190, 229	67 09.057	-135 41.121	5.9	288	6 – 10 ^d
HB	190, 229	67 14.397	-135 49.167	13.6 ^c	257	6 – 10 ^d
HC	190, 229	67 19.652	-135 53.620	10.3, 10.3 ^c	408	6 – 10 ^d
HD	190, 229	67 24.025	-135 20.048	1.8	137	6 – 10 ^d
Weather Station		67 14.756	-135 12.920			

1126
 1127 ^a Excludes samples for the FM3 ‘environmental controls’ analysis which was conducted on 17 additional
 1128 dates; HD, Julian date 229 did not include a within-slump sample.
 1129 ^b The length of debris tongue measured from the base of the debris scar, along the valley bottom stream
 1130 ^c Site HB is comprised of two smaller slump features that have merged into the scar zone delineated
 1131 here; site HC is comprised of 5 separate slump features that have merged into two scar zones, each with
 1132 an area of 10.3 ha
 1133 ^d Rough estimates by field crews over 2014 and 2015 field seasons
 1134 ^e Kokelj et al. 2015
 1135
 1136
 1137

1138 **Table 2:** Results of the mixed-effects models used to assess the effects of slumping on stream water
 1139 chemistry and optical characteristics. Downstream models incorporated data from downstream and
 1140 upstream sites; within-slump models incorporated data from within-slump and upstream sites. Provided
 1141 are degrees of freedom (df), t-statistics, and p-values for individual model runs. Further details on the
 1142 statistical approach are provided in Section 3.4.
 1143

	Downstream			Within-slump		
	df	t	p	df	t	p
DOC	20	-12.895	<.0001	30	-1.468	0.153
Na	33	9.662	<.0001	30	7.278	0.000
Ca	33	9.767	<.0001	30	4.782	0.000
Mg	33	6.166	<.0001	30	8.593	0.000
Conductivity	32	43.083	<.0001	30	11.895	0.000
TSS	29	6.692	<.0001	28	2.187	0.037
SUVA	32	-4.460	<.0001	30	-35.052	0.000
S _R	32	5.333	<.0001	31	8.065	0.000
S ₂₇₅	31	2.856	0.008	31	8.159	0.000
S ₃₅₀	32	-2.196	0.036	31	16.665	0.000

1144

1145

1146 **Table 3:** Measured fraction modern carbon (F^{14C}) and estimated calendar years before present for 14C of
 1147 dissolved organic carbon samples collected upstream of, and within drainage waters of, selected slump
 1148 sites. Data were collected during the summer of 2016. nc indicates sample not collected. Error
 1149 estimates indicate 1σ .

1150

Site	F^{14C}		14C yr BP	
	Upstream	Within-slump	Upstream	Within-slump
FM4	0.9734 ± 0.0029	nc	217 ± 24	nc
FM2	0.9764 ± 0.0032	0.3030 ± 0.0024	192 ± 27	9592 ± 64
FM3	1.0023 ± 0.0030	0.3618 ± 0.0018	modern	8167 ± 39
SD	1.0216 ± 0.0035	0.8659 ± 0.0025	modern	1157 ± 23

1151

1152

1153 **Table 4:** Results of multiple linear regression analyses to assess environmental controls on upstream and downstream DOC flux, and upstream
 1154 and downstream DOC concentration. nr indicates variables that were not retained in the best fit regression model; NA indicates variables that
 1155 were not run in individual analyses. Significant p-values are indicated with bold text; marginal results ($0.05 < p < 0.10$) are indicated in italics.
 1156 Model statistics are as follows: downstream flux $r^2=0.84$, $F_{7,11}=8.25$, $p = 0.001$; upstream flux $r^2=0.87$, $F_{7,11}=10.79$, $p < 0.001$; downstream
 1157 concentration $r^2=0.85$, $F_{4,14}=19.57$, $p < 0.001$; upstream concentration $r^2=0.91$, $F_{5,13}=27.05$, $p < 0.001$.

Coefficient	Downstream DOC flux			Upstream DOC flux			Downstream DOC concentration			Upstream DOC concentration		
	Estimate	t	p	Estimate	t	p	Estimate	t	p	Estimate	t	p
Average Air Temperature (°C)												
0 h	-67.08	-1.685	0.120	-115.96	-3.286	0.007	nr	nr	nr	0.165	2.349	0.035
48 h	nr	nr	nr	56.32	1.534	0.153	0.332	6.886	<0.001	0.396	5.510	<0.001
72 h	-95.15	-2.594	0.025	-94.17	-2.717	0.020	nr	nr	nr	nr	nr	nr
120 h	nr	nr	nr	nr	nr	nr	0.134	3.527	0.003	0.203	4.411	<0.001
Rainfall (mm)												
0h	116.13	5.411	<0.001	105.47	6.039	<0.001	<i>-0.066</i>	<i>-1.967</i>	<i>0.069</i>	nr	nr	nr
48h	nr	nr	nr	nr	nr	nr	nr	nr	nr	nr	nr	nr
72h	nr	nr	nr	nr	nr	nr	nr	nr	nr	nr	nr	nr
120h	<i>-23.94</i>	<i>-1.970</i>	<i>0.075</i>	-24.15	-2.529	0.028	nr	nr	nr	nr	nr	nr
Average net radiation (W m⁻²)												
0h	4.96	1.286	0.225	nr	nr	nr	-0.021	-4.043	0.001	-0.021	-3.387	0.005
48h	nr	nr	nr	nr	nr	nr	nr	nr	nr	nr	nr	nr
72h	5.58	1.545	0.151	4.04	1.563	0.146	nr	nr	nr	nr	nr	nr
120h	nr	nr	nr	nr	nr	nr	nr	nr	nr	nr	nr	nr
Total suspended solids (mg L⁻¹)												
Downstream	<i>-0.02</i>	<i>-2.102</i>	<i>0.059</i>	NA	NA	NA	nr	nr	nr	NA	NA	NA
Upstream	NA	NA	NA	<i>-0.32</i>	<i>-1.626</i>	<i>0.132</i>	NA	NA	NA	<i>-0.0006</i>	<i>-1.627</i>	<i>0.128</i>

1158

1159 **Figure captions:**

1160 **Fig. 1:** Location and morphology of thaw slumps on the Peel Plateau, Northwest Territories, Canada.
1161 Panel A depicts the stream networks and location of the eight retrogressive thaw slumps studied. Panel
1162 B depicts representative sampling locations at each slump site; FM3 depicted. Panels C-E depict
1163 representative thaw-slump headwall stratigraphies. Panel C shows a mega-slump (FM3, the smallest
1164 mega-slump, is depicted); panel D shows a moderate-sized slump (HB); panel E shows the smallest
1165 slump that was sampled (SD). In panels C and D, the approximate location of the modern active layer (a),
1166 early Holocene-aged relict active layer (b), and Pleistocene-aged glacial materials (c) is shown. Photo
1167 credit: Scott Zolkos.

1168 **Fig. 2:** The effect of retrogressive thaw slumps on stream water dissolved organic carbon (DOC)
1169 concentration. Each data point represents the mean and standard error of measurements across all
1170 sampling dates, as described in Table 1. The bottom two panels show the ratio of within-slump:
1171 upstream, and downstream: upstream DOC concentrations within individual slumps, with points
1172 indicating the mean and standard error of this ratio across sample dates.

1173 **Fig. 3:** Box and whisker plots to illustrate the effects of retrogressive thaw slump activity on stream
1174 geochemistry. Each boxplot includes data from across all slumps and sampling periods, and indicates
1175 median values, 25th and 75th percentiles (box extremities), 10th and 90th percentiles (whiskers), and
1176 outlier points. U=upstream sites; W=within-slump sites; D=downstream sites.

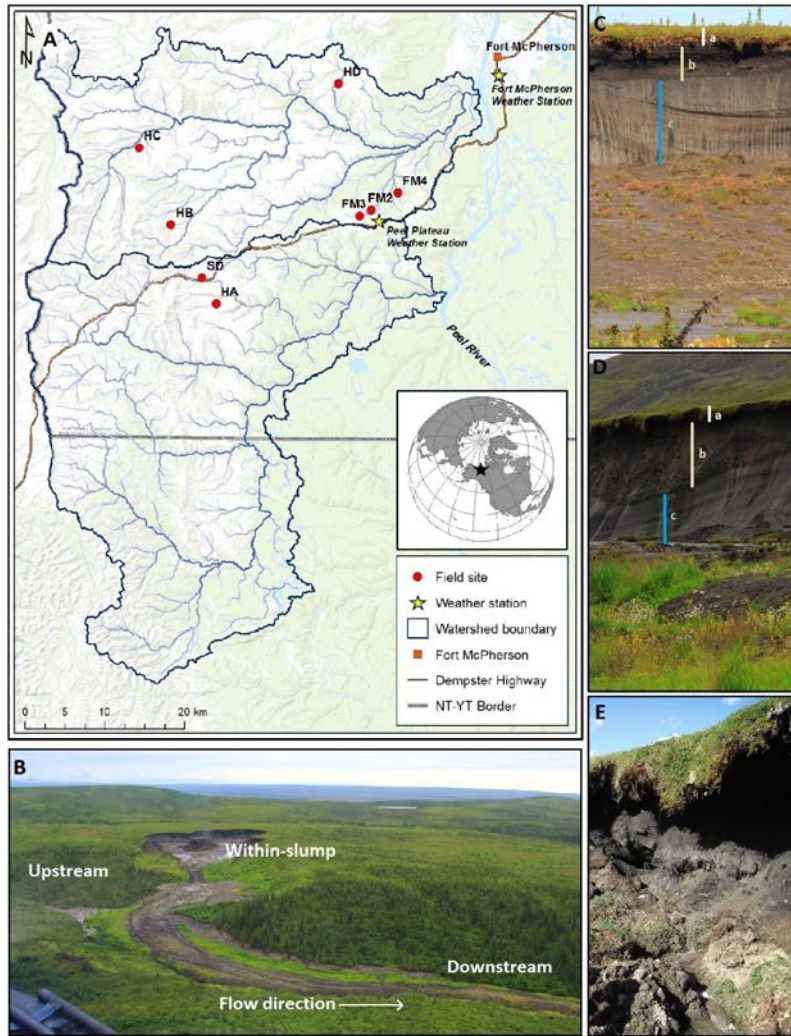
1177 **Fig. 4:** The effect of retrogressive thaw slumps on the optical properties of stream water dissolved
1178 organic matter. Each data point represents the mean and standard error of measurements across all
1179 sampling dates, as described in Table 1. Shown are specific UV absorbance (SUVA₂₅₄), spectral slopes
1180 between 275-295 and 350-400 nm (S₂₇₅₋₂₉₅; S₃₅₀₋₄₀₀) and the slope ratio (S_R).

1181 **Fig. 5:** Paired oxygen isotopic ($\delta^{18}\text{O}$ ‰) and SUVA₂₅₄ (L mg C⁻¹m⁻¹) data, to demonstrate the relationship
1182 between source water age and dissolved organic matter composition. Reference $\delta^{18}\text{O}$ values are from
1183 Lacelle et al. (2013): the modern active layer value is derived from active layer pore water in this region,
1184 icy diamicton has been sourced as Holocene in origin, and the $\delta^{18}\text{O}$ value for Pleistocene-aged ground ice
1185 is the most positive value for this region.

1186 **Fig. 6:** Environmental conditions (solar radiation, precipitation and mean daily air temperature) and DOC
1187 flux upstream and downstream of slump FM3 across a month-long sample period (July 12-August 12,
1188 2014). Corresponding multiple linear regressions are described in Table 4.

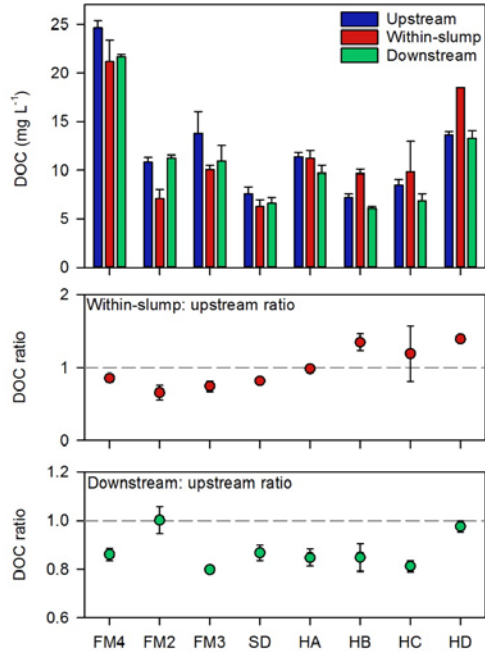
1189 **Fig. 7:** Within-slump fluxes of dissolved organic carbon (DOC), and TSS, compared to the calculated
1190 (downstream - upstream) fluxes for these two constituents. TSS – a conservative tracer over short
1191 distances – shows an additive response where the measured within-slump flux is equivalent to the
1192 calculated (downstream - upstream) flux. In contrast, DOC shows clear evidence of downstream loss.

1193



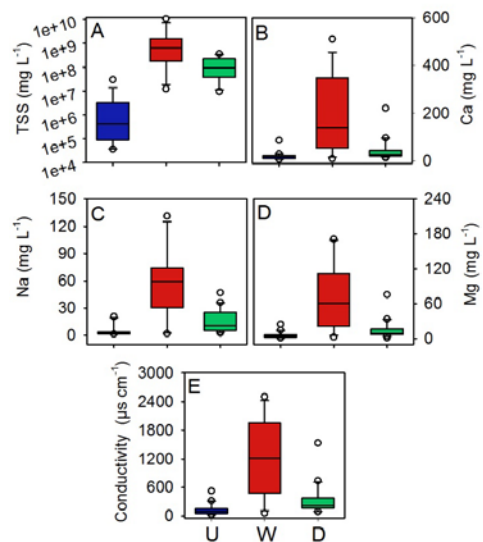
1194
 1195 **Fig. 1:** Location and morphology of thaw slumps on the Peel Plateau, Northwest Territories, Canada.
 1196 Panel A depicts the stream networks and location of the eight retrogressive thaw slumps studied. Panel
 1197 B depicts representative sampling locations at each slump site; FM3 depicted. Panels C-E depict
 1198 representative thaw-slump headwall stratigraphies. Panel C shows a mega-slump (FM3, the smallest
 1199 mega-slump, is depicted); panel D shows a moderate-sized slump (HB); panel E shows the smallest
 1200 slump that was sampled (SD). In panels C and D, the approximate location of the modern active layer (a),
 1201 early Holocene-aged relict active layer (b), and Pleistocene-aged glacigenic materials (c) is shown. Photo
 1202 credit: Scott Zolkos.

1203
1204
1205



1206 **Fig. 2:** The effect of retrogressive thaw slumps on stream water dissolved organic carbon (DOC)
1207 concentration. Each data point represents the mean and standard error of measurements across all
1208 sampling dates, as described in Table 1. The bottom two panels show the ratio of within-slump:
1209 upstream, and downstream: upstream DOC concentrations within individual slumps, with points
1210 indicating the mean and standard error of this ratio across sample dates.

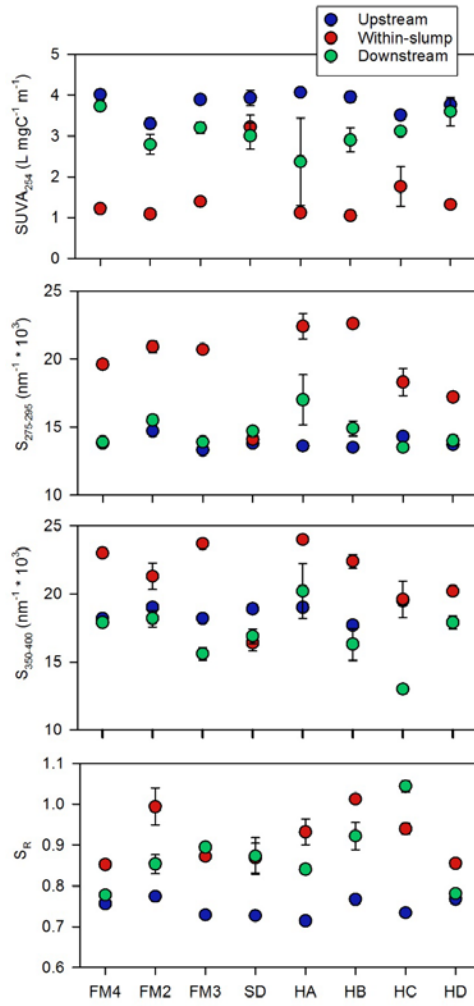
1211



1212

1213 **Fig. 3:** Box and whisker plots to illustrate the effects of retrogressive thaw slump activity on stream
 1214 geochemistry. Each boxplot includes data from across all slumps and sampling periods, and indicates
 1215 median values, 25th and 75th percentiles (box extremities), 10th and 90th percentiles (whiskers), and
 1216 outlier points. U=upstream sites; W=within-slump sites; D=downstream sites.

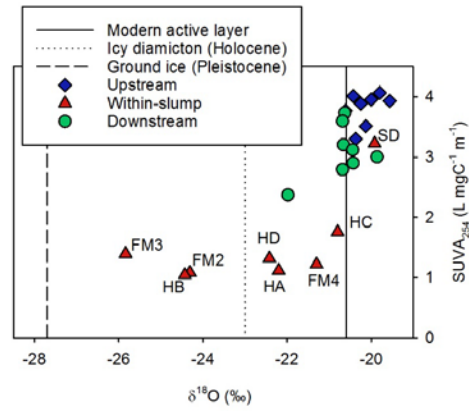
1217



1219 **Fig. 4:** The effect of retrogressive thaw slumps on the optical properties of stream water dissolved
 1220 organic matter. Each data point represents the mean and standard error of measurements across all
 1221 sampling dates, as described in Table 1. Shown are specific UV absorbance (SUVA₂₅₄), spectral slopes
 1222 between 275-295 and 350-400 nm (S₂₇₅₋₂₉₅; S₃₅₀₋₄₀₀) and the slope ratio (S_R).

1223

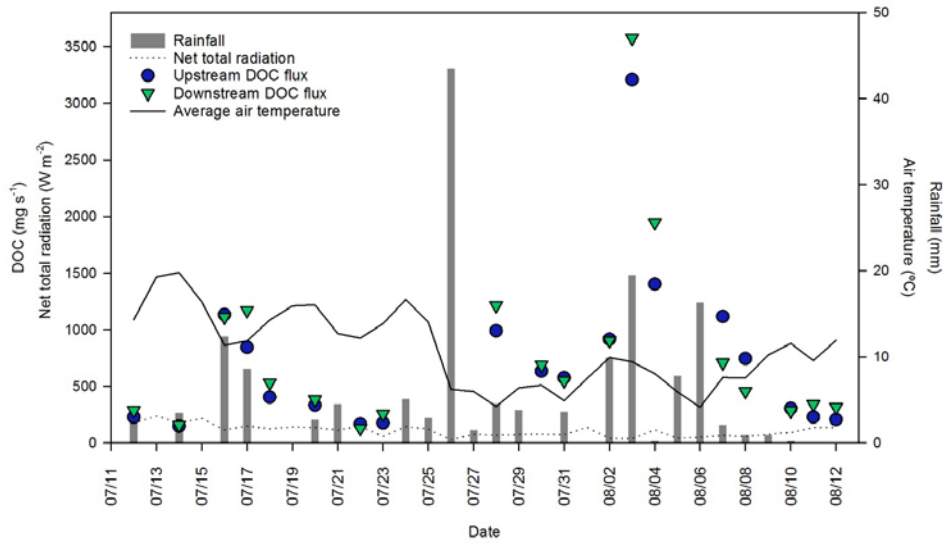
1224



1225 **Fig. 5:** Paired oxygen isotopic ($\delta^{18}\text{O}$ ‰) and SUVA₂₅₄ ($\text{L mg C}^{-1}\text{m}^{-1}$) data, to demonstrate the relationship
1226 between source water age and dissolved organic matter composition. Reference $\delta^{18}\text{O}$ values are from
1227 Lacelle et al. (2013): the modern active layer value is derived from active layer pore water in this region,
1228 icy diamicton has been sourced as Holocene in origin, and the $\delta^{18}\text{O}$ value for Pleistocene-aged ground ice
1229 is the most positive value for this region.

1230

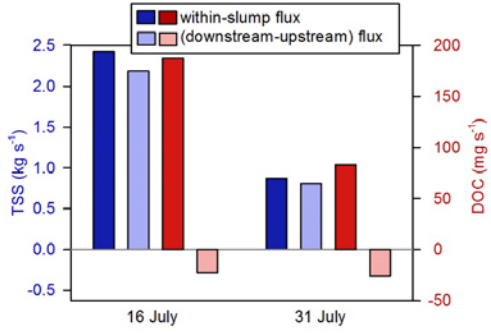
1231



1232 **Fig. 6:** Environmental conditions (solar radiation, precipitation and mean daily air temperature) and DOC
1233 flux upstream and downstream of slump FM3 across a month-long sample period (July 12-August 12,
1234 2014). Corresponding multiple linear regressions are described in Table 4.

1235

1236



1237

1238 **Fig. 7:** Within-slump fluxes of dissolved organic carbon (DOC), and TSS, compared to the calculated
1239 (downstream - upstream) fluxes for these two constituents. TSS – a conservative tracer over short
1240 distances – shows an additive response where the measured within-slump flux is equivalent to the
1241 calculated (downstream - upstream) flux. In contrast, DOC shows clear evidence of downstream loss.

1242

1243

